DMD Fast Forward. Published on July 2, 2020 as DOI: 10.1124/dmd.120.000096
This article has not been copyedited and formatted. The final version may differ from this version.

# Bioactivation of α,β-Unsaturated Carboxylic Acids Through Acyl Glucuronidation

Teresa Mulder, Sudheer Bobba, Kevin Johnson, Jessica M. Grandner, Wei Wang, Chenghong Zhang, Jingwei Cai, Edna F. Choo, S. Cyrus Khojasteh, Donglu Zhang

Affiliation: Drug Metabolism and Disposition (TM, SB, KJ, WW, CZ, JC, EFC, SCK, DZ), Discovery Chemistry (JMG), Genentech, 1 DNA Way, South San Francisco, CA 94080

DMD Fast Forward. Published on July 2, 2020 as DOI: 10.1124/dmd.120.000096
This article has not been copyedited and formatted. The final version may differ from this version.

**Running title: Acyl glucuronidation activates unsaturated carboxylic acids**

Corresponding author:

Drug Metabolism and Pharmacokinetics, Genentech, 1 DNA Way, South

San Francisco, CA 94080. zhang.donglu@gene.com

Number of Table: 2

Number of Figures: 7 Number

of references: 37

Number of words in sections:

Abstract: 242

Introduction: 306

Results:

Discussion: 1400

**Abbreviations:**

adenosine monophosphate (AMP), Cynomolgus Monkey Liver Microsomes (CLM), Coenzyme A (CoA), Collision-Induced Dissociation (CID), Density Functional Theory (DFT), Dulbecco Modified Eagle Medium (DMEM), Estrogen Receptor (ER), Selective Estrogen Receptor Alpha (ERα), Estrogen Receptor-Positive (ER+), Glutathione (GSH), glutathione transferase (GST); Heated-Electrospray Ionization (H-ESI), Higher Energy Collisional Dissociation (HCD), Human Liver Microsomes (HLM), High-Performance Liquid Chromatography (HPLC), Liquid Chromatography / Mass Spectrometry (LC/MS), Liquid Chromatography with Tandem Mass Spectrometry (LC-MS/MS), Liquid Scintillation Counting (LSC), Lowest Unoccupied Molecular Orbital (LUMO), Multiple Reaction Monitoring (MRM), Mass Spectrometry (MS), Tandem Mass Spectrometry (MS/MS), Reduced Nicotinamide Adenine Dinucleotide Phosphate (NADPH), Selective Estrogen Receptor Degrader (SERD)

DMD Fast Forward. Published on July 2, 2020 as DOI: 10.1124/dmd.120.000096
This article has not been copyedited and formatted. The final version may differ from this version.

## Abstract

Following oral administration of [$^{14}$C]**GDC-0810**, an α,β-unsaturated carboxylic acid, to monkeys, unchanged parent and its acyl glucuronide metabolite, **M6,** were the major circulating drug-related components. In addition, greater than 50% of circulating radioactivity in plasma was found to be non-extractable 12 hours post-dose, suggesting possible covalent binding to plasma proteins. In the same study, one of the minor metabolites was a cysteine conjugate of **M6** (**M11**) that was detected in plasma and excreta (urine and bile). The potential mechanism for the covalent binding to proteins was further investigated using *in vitro* methods. In incubations with GSH or cysteine (5mM), GSH- and cysteine-conjugates of **M6** were identified, respectively. The cysteine reaction was efficient with a half-life of 58.6 min ($k_{react}$ = 0.04 1/M/sec). Loss of 176 Da (glucuronic acid) followed by 129 Da (glutamate) in mass fragmentation analysis of the GSH-adduct of **M6** (**M13**) suggested the glucuronic acid moiety was not modified. The conjugation of N-glucuronide **M4** with cysteine in buffer was >1000-fold slower than with **M6**. Incubations of **GDC-0810**, **M4**, or **M6** with monkey or human liver microsomes in the presence of NADPH and GSH did not produce any oxidative GSH adducts, and the respective substrates were qualitatively recovered. *In silico* analysis quantified the inherent reactivity differences between the glucuronide and its acid precursor. Collectively, these results show that acyl glucuronidation of α,β-unsaturated carboxylic acids can activate the compound towards reactivity with GSH, cysteine, or other biologically occurring thiols, and should be considered during the course of drug discovery.

Significance statement:

Acyl glucuronidation of the α,β-unsaturated carboxylic acid in GDC-0810 activates the conjugated alkene towards nucleophilic addition by GSH or other reactive thiols. This is the first example that a bioactivation mechanism could lead to protein covalent binding to α,β-unsaturated carboxylic acid compounds.

DMD Fast Forward. Published on July 2, 2020 as DOI: 10.1124/dmd.120.000096
This article has not been copyedited and formatted. The final version may differ from this version.

## Introduction

Approximately 80% of all breast cancers express and are dependent on the estrogen receptor (ER) for tumor growth and progression (Jemal et al., 2011). Despite the effectiveness of available hormonal therapies such as tamoxifen, aromatase inhibitors (e.g. anastrozole, letrozole, and exemestane), and full ER antagonists/degraders (e.g. fulvestrant), many patients develop resistance to these agents and, hence, require further treatment (Di Leo et al., 2010; Baselga et al., 2012; Miller et al., 2010; Van Tine et al., 2012). **GDC-0810** (Figure 1), an α,β-unsaturated carboxylic acid, is a novel, selective estrogen receptor alpha (ERα) antagonist and inducer of ERα degradation, which has potential to be used as an oral anticancer drug for estrogen receptor-positive (ER+) breast cancer as either a single agent or in combination with other anti-cancer drugs.

While investigating **GDC-0810** as a candidate molecule, several *in vivo* PK and metabolism studies were performed. Radioactivity extraction recovery was low (<50%) in plasma of monkeys following oral administration of [$^{14}$C]**GDC-0810**. Extensive organic extraction of plasma proteins suggested that the radioactivity was covalently bound to proteins. In monkey plasma, the identification of **M11**, the cysteine conjugate of **M6**, provided us with a clue that a nucleophile could form an adduct with **M6** through Michael addition to the β-carbon of the major circulating metabolite. To further elucidate the mechanism for the protein covalent binding, *in vitro* experiments were conducted to answer these questions: (1) How efficient is the Michael addition of a nucleophile to the major circulating metabolite **M6**? (2) Does Michael addition occur for **GDC-0810** or other metabolites? (3) Was there any direct replacement of the acyl glucuronide by a nucleophile? (4) Was a Schiff base formed with an amino group from an acyl-migration product, leading to formation of an adduct? (5) Was there any bioactivation by P450 enzymes to form reactive metabolites that could be trapped by GSH? (6) Was any AMP

DMD Fast Forward. Published on July 2, 2020 as DOI: 10.1124/dmd.120.000096
This article has not been copyedited and formatted. The final version may differ from this version.

or CoA adduct formed in hepatocyte incubations? Herein, we discuss these experiments and findings that can be related to protein covalent binding.

## Materials and Methods

### Chemicals and Reagents

**GDC-0810**, its acyl glucuronide (**M6**) and its *N*-glucuronide (**M4**) were synthesized and characterized at Genentech (South San Francisco, CA). [$^{14}$C]**GDC-0810** was synthesized by Selcia (Essex, UK) with the specific radioactivity of 8.8 kBq/mg.

Liver microsomal preparations and cryopreserved hepatocytes were purchased from In Vitro Technologies (Melbourne, AU). Acetonitrile and methanol were purchased from EMD Chemicals (Gibbstown, NJ). Ultrapure HPLC water and formic acid were purchased from J.T. Baker (Center Valley, PA). Ammonium formate and ammonium hydroxide solution were purchased from Fluka (St. Louis, MO). Sodium citrate, GSH, cysteine, and other chemicals were purchased from Sigma-Aldrich (St. Louis, MO).

### Monkey plasma collection, extraction, and metabolite profiling

Plasma samples were collected from cynomolgus monkeys following 50 mg/kg oral administration of [$^{14}$C]**GDC-0810**. Approximately 1.5 g of each plasma sample was treated with 3x volume of 0.1% formic acid in acetonitrile for protein precipitation. Samples were then mixed by vortex for 5 min and sonicated for 10 min at room temperature. Supernatants were transferred to a new set of tubes following centrifugation at 2700 □ *g* for 30 min. Extraction recoveries were determined by liquid scintillation counting (LSC). The sample-extraction recovery of radioactivity was assessed by comparing the total radioactivity in the processed samples with the total radioactivity in un-precipitated plasma. Following extraction, the weight of the supernatant was measured and an aliquot of the supernatant was counted for radioactivity. The total radioactivity of the processed samples was calculated using radioactivity of an aliquot measured by LSC, aliquot weights, and supernatant weights.

DMD Fast Forward. Published on July 2, 2020 as DOI: 10.1124/dmd.120.000096
This article has not been copyedited and formatted. The final version may differ from this version.

Supernatant was evaporated to near-dryness using a SpeedVac concentrator, and reconstituted with 300 µL water:acetonitrile (2:1, v/v). The samples were sonicated, mixed, and analyzed by LC-MS. Radioactivity was analyzed by scintillation counting. The extensively washed protein pellets were analyzed by LSC after oxidizer treatment.

In vivo sample analysis was performed on an HPLC system consisting of Dionex Ultimate 3000 RS pumps, and a Diode Array Detector coupled with either a Lumos Orbitrap or a Q Exactive Plus mass spectrometer (ThermoFisher Scientific, San Jose, CA). Liquid chromatography was performed with a Polaris C18-A column, 4.6 x 150 mm, 3 µ m (Agilent Technologies, Santa Clara, CA) with mobile phases 10 mM ammonium acetate in water with 0.1% formic acid (mobile phase A) and acetonitrile (mobile phase B). The flow rate was 1 ml/min with 10:1 post column split. The HPLC gradient was as follows: initial hold at 5% B for 2 min, ramp to 40% B at 15 min, hold at 40% B until 28 min, ramp to 50% B at 28.1 min, hold at 50% B until 50 min, and then ramp to 95% B at 54 min, hold until 57 min and return to initial equilibrium conditions. Electrospray ionization was used with electrospray voltage set at 4.0 kV and a capillary temperature of 270$^{o}$C. The full-scan mass spectra were obtained at resolving power of 30,000 with accurate mass measurements using external calibration. The corresponding data dependent tandem mass spectrometry (MS/MS) scans acquired at a resolving power of 7,500 with collision induced dissociation.

**Product identification in Incubations of GDC-0810, M4, and M6 in buffer with GSH or cysteine**

Incubations were carried out in 100 mM potassium phosphate buffer (pH 7.4) with either 1 mM cysteine or glutathione. **GDC-0810**, **M6** or **M4** at 5 µ M (< 0.1% DMSO final) were incubated in buffer alone or buffer with 1 mM cysteine or glutathione for 1 hour at 37$^{o}$C in a shaking water bath (120 rpm). Incubations were quenched on ice. Samples were injected onto a Q Exactive Plus mass spectrometer connected to a Dionex HPLC (ThermoFisher Scientific, San Jose, CA). Mass spectrometry full scan and MS$^{2}$ modes were collected. H-ESI ion source was used on the MS in positive mode with a spray voltage of 3500 eV, probe heater temp of 425$^{o}$C. HCD collision energy used for MS$^{2}$ was 25-45. The LC separation used a phenylhexyl 100 x 2.1 mm, 1.7 µ column

DMD Fast Forward. Published on July 2, 2020 as DOI: 10.1124/dmd.120.000096
This article has not been copyedited and formatted. The final version may differ from this version.

(Phenomenex, Torrence, CA) with a 0.4 ml/min flow rate of water with 0.1% formic acid (mobile phase A) and acetonitrile with 0.1% formic acid (mobile phase B). The gradient used was: initial hold at 2% B for 1 min, ramp to 95% B at 12.5 min, hold until 13 min and return to initial equilibrium conditions.

**Product identification in incubations of GDC-0810, M4, and M6 in liver microsomes with NADPH and GSH**

**GDC-0810**, **M6**, or **M4** (5 µ M) was incubated in HLM or CLM (0.5 mg/ml) in 100 mM potassium phosphate buffer (pH7.4) and GSH (5 mM) in the presence or absence of NADPH (1 mM). After the reaction was complete within an hour, the mixture was quenched with 3 volumes of cold acetonitrile:methanol (9:1) and chilled on ice for 30 min. The resulting suspension was centrifuged at 3000 x*g* for 30 min and supernatant was concentrated under nitrogen. Samples were analyzed on a Thermo Fusion Lumos mass spectrometer (ThermoFisher Scientific, San Jose, CA) coupled with a Kinetex C18-XB
100 x 2.1 mm, 1.7 µm, 100Å column (Phenomenex, Torrence, CA). LC mobile phase containing 0.1% formic acid in water (A) vs 0.1% formic acid in acetonitrile (B) was used as a gradient as follows: initial hold at 5% B for 3 min, ramp to 50% B at 15 min, ramp to
95 % B at 18 min, hold for 4 min, and return to initial equilibrium conditions.

**Cysteine reactivity in incubations of GDC-0810, M4, and M6 in buffer with cysteine**

**GDC-0810**, **M6**, and **M4** at 1 µ M were incubated with 5 mM cysteine in 100 µ L of 100 mM phosphate buffer pH 7.4 for 0, 30, 60, 90, 120, 150, and 180 min at 37$^{o}$C in Eppendorf tubes with 800 RPM shaking. The samples were analyzed by Sciex TripleQ 5500 LCMS/MS analysis with multiple-reaction monitoring in positive mode. The samples were quenched with 100 µ L of cold acetonitrile containing two Internal Standards (pre-IS: diphenhydramine and post-IS: propanolol) and injected (10 µ L) at real time. The % remaining of parent was plotted against time. Slope and $t_{1/2}$ were

DMD Fast Forward. Published on July 2, 2020 as DOI: 10.1124/dmd.120.000096
This article has not been copyedited and formatted. The final version may differ from this version.

calculated by GraphPad. Acrylamide-containing neratinib and acalabutinib were included as positive controls for the cysteine reactivity determination.

**Metabolite formation of GDC-0810 in hepatocytes of human and monkey**

**GDC-0810** at 1 µ M was incubated with cryopreserved hepatocytes of human, and monkey (0.5 million cells/mL) for 3 h at 37$^{o}$C in DMEM buffer. The samples were analyzed by LC-MS/MS analysis on QE plus (ThermoFisher Scientific, San Jose, CA). LC mobile phase containing 0.1% formic acid in water vs acetonitrile was used as a gradient on Kinetex C18 1.7 µm, 100Å, 100 x 2.1 mm column (Phenomenex, Torrence, CA). Full scan and MS/MS scans in positive mode were collected to detect metabolites of glucuronide (*m/z* 623.1591), adducts of CoA (*m/z* 1196.2317), adenosine monophosphate (AMP) (*m/z* 776.1796), conjugates of taurine (*m/z* 554.1311) or glycine (*m/z* 504.1485), as well as conjugates of the acyl glucuronide with GSH (*m/z* 930.2429) or cysteine (*m/z* 744.1788).

**Quantum mechanical methods**

The model compounds cinnamic acid and its O-glucuronide were used for this analysis. Conformers of the O-glucuronide (**B**) were generated using the “conformer distribution” functionality within Spartan ’18 (Wavefunction, Inc., Irvine, CA) with the software’s implementation of MMFF (Halgren, 1996a-d; Halgren and Nachbar, 1996). Conformers were then exported and geometry otimizations were run with Gaussian09 (Revision E.01, Gaussian Inc., Wallingford CT, 2013; see supplemental information for full reference). Initial geometry optimizations of the conformers of **B** were run at the HF (Roothaan, 1951; Cossi et al., 2003) level with the 6-31G(d) basis set and implicit CPCM (Barone and Cossi, 1998) solvent model for water. These initial geometry optimizations were used to identify the lowest energy conformers for further optimization at higher levels of theory. The top two conformers of **B** and the sole conformer of cinnamic acid (**A**) were then optimized at the M06-2X (Zhao and Truhlar, 2008) level of theory with the 6-31+G(d) basis set and implicit CPCM solvent model for water. The lowest energy conformer of **B** and **A** were then subjected to a single point calculation within Spartan ’18 (Q-Chem implementation within Spartan ’18: Shao et al., 2015) at the M06-2X level

DMD Fast Forward. Published on July 2, 2020 as DOI: 10.1124/dmd.120.000096
This article has not been copyedited and formatted. The final version may differ from this version.

of theory with the 6-311+G(2df,2p) basis set and the implicit CPCM solvent model for water (Table S2). 3D rendering of the LUMO of **B** was made within Spartan '18.

## Results

### Metabolic pathways of GDC-0810 in monkeys

The major clearance pathway of **GDC-0810** in monkeys was through acyl glucuronidation with **M6** as the major metabolite in plasma, bile, and urine (Table 2, supplemental Figures S1 and S2). Other metabolites identified in monkey plasma and excreta include di-glucuronide (**M1**), oxidative di-glucuronide (**M3**), di-glucuronide (**M4**), oxidative glucuronide (**M5**), oxidative metabolite (**M7**), and cysteine adduct of **M6 (M11).** , The radioactivity extraction recoveries from monkey plasma decreased from 82% at
3 h to less than 50% at 24 h and to a lower recovery at later time points post-dose (Table 1). The extraction recovery was approximately 75% from 0-168 h fecal samples. Subsequent oxidation of the protein precipitate pellet showed that the unextractable radioactivity was associated with the pellet from plasma samples. The mass balance as well as metabolites identified in plasma, urine, bile, and feces of monkeys following oral administration of [$^{14}$C]**GDC-0810** are included in the Supplemental Information. The radioactive metabolite profiles of **GDC-0810** in monkey urine, bile, and feces are also shown in the supplemental information (Figure S2 and Table S1).

There were two metabolites (**M6** and **M11**) in plasma extract that were of particular interest. The radioactive peak of **M6** (m/z 623) was a major circulating metabolite (Figure 2). The MS/MS spectra showed product ions at *m/z* 605 (loss of $H_2O$), 447 (loss of anhydro-glucuronic acid), 299 (loss of phenyl propenoic acid), and 311 (loss of indazole and $H_2O$). The elemental composition of **M6** was confirmed using accurate mass analysis. The fragmentation pattern of **M6** observed in study samples was similar to that of the standard (Figure S3).

The radioactive peak of **M11** (m/z 744) was observed in monkey plasma as well as in urine and bile. The mass spectra showed product ions at *m/z* 726 (loss of $H_2O$), 623

DMD Fast Forward. Published on July 2, 2020 as DOI: 10.1124/dmd.120.000096
This article has not been copyedited and formatted. The final version may differ from this version.

(loss of cysteine), 568 (loss of anhydro-glucuronic acid), and 447 (loss of anhydro-glucuronic acid and cysteine). The elemental composition of **M11** was confirmed by accurate mass analysis (Figure 3). Based on these fragmentation data, **M11** was tentatively assigned as the cysteine adduct of **GDC-0810** glucuronide **M6**. The assignment of **M11** was further confirmed by *in vitro* incubation of **M6** with cysteine in buffer.

**Adduct formation of GDC-0810, M6, and M4 *in vitro***

**GDC-0810**, along with its glucuronide metabolites (**M4** and **M6**), were individually incubated in phosphate buffer in the presence of cysteine or GSH to examine the potential for chemical reactivity. After analysis via LC-MS, no GSH (+307 Da) or cysteine (+121 Da) adducts were detected for **GDC-0810** (Figure 4A). Similar results were observed after incubation of the *N*-glucuronide metabolite **M4**, with no GSH adduct and a very low abundance of cysteine adduct observed (>1000-fold less). Conversely, the GSH conjugates of the glucuronide metabolite **M13** (M+307 of **M6**) were relatively abundant in the GSH incubation (Figure 4C). This was also observed with the corresponding cysteine conjugate (M+121 of **M6**, **M11**) in the cysteine incubation (Figure 4B). Acyl-migration for **M6** is likely responsible for the peaks with the same *m/z* or its cysteine conjugate in the **M6** incubations. These results suggest that the chemical reactivity of the acyl *O*-glucuronide **M6** is much higher than that of **GDC-0810** or its *N*-glucuronide metabolite **M4**. For acyl glucuronide **M6,** time-dependent acyl migration was observed. Two cysteine conjugate peaks observed for **M11** are likely a result of acyl-migration isomers. Only one peak observed in vivo plasma could be a result of less acyl migration in the plasma or a co-elution under the LC method used. The broader **M13** peak formed from the reaction of **M6** with GSH could result from co-eluting peaks.

The structural proposal of **M13** (*m/z* 930) is supported by LC-MS/MS fragmentation data (Figure 5). Fragmentation was conducted by collision-induced dissociation (CID) and higher energy collisional dissociation (HCD) to characterize GSH conjugates. Fragment ions of *m/z* 801 and *m/z* 625 resulted from neutral loss of γ-glutamate (129 Da) and subsequent neutral loss of glucuronide moiety (176 Da), respectively. Ions *m/z* 754 and *m/z* 447 result from neutral losses of glucuronide (176 Da) and glucuronide+GSH

DMD Fast Forward. Published on July 2, 2020 as DOI: 10.1124/dmd.120.000096
This article has not been copyedited and formatted. The final version may differ from this version.

moieties (176+307 Da). Fragment ions *m/z* 405 and *m/z* 299 suggested the addition of GSH on the allyl group, supporting the stability of **GDC-0810** aromatic ring system.

The Michael addition of cysteine to **M6** to form **M11** was efficient with a half-life of 58 min. For comparison, $k_{react}$ (in $M^{-1}s^{-1}$; t1/2 in min) were 0.043 (26.8), 0.0077 (149.8) for the two acrylamide-containing drugs neratinib and acalabutinib, respectively.

**M13** formed in situ was subject to glucuronidase treatment and the GSH adduct of **GDC-0810** (**M14**) was identified as a product of the enzymatic incubation (Figure S4). The results suggested that the Michael addition product was stable even after removal of the glucuronic acid group and provides further evidence that the formation of **M13** is from **M6** rather than from **GDC-0810**. The **M14** (*m/z* 754) LC-MS/MS fragmentation pattern also suggests the addition of GSH on the allyl group due to fragment ions *m/z* 405 and *m/z* 299 (Table 1). Double-charged fragment ion *m/z* 340 resulted from neutral loss of glycine (75 Da), and ion *m/z* 447 resulted from neutral loss of GSH moiety (307 Da).

**GDC-0810** and its glucuronide metabolites (**M4** and **M6**), were also incubated in monkey or human liver microsomes in the presence NADPH and GSH to examine the potential for P450-mediated bioactivation and reactive metabolite formation. LC-MS showed that no GSH (M+307 or 305) adducts were detected for **GDC-0810** or **M4** (Figure 6A and 6C). For **M6**, although the GSH conjugate **M13** (M+307) was the major product, there were no adducts resulting from oxidative metabolites [M+16(32)+305(307)] (Figure 6B) from these incubations.

## Metabolite formation of GDC-0810 in hepatocytes

Full scan and MS/MS scan analysis showed that **M6** and **M4** were prominent metabolites in incubations of GDC-0810 with human and monkey hepatocytes. No CoA or AMP adduct were identified. Taurine or glycine adducts as well as cysteine or GSH conjugates of **M6** were also not identified.

## Quantum mechanical calculations

Acids, in general, are weaker electrophiles than esters. This is due to the significant electron density of the carboxylate, hindering addition of an electron-rich nucleophile.

DMD Fast Forward. Published on July 2, 2020 as DOI: 10.1124/dmd.120.000096
This article has not been copyedited and formatted. The final version may differ from this version.

The weaker reactivity of acids applies to both 1,2-addition to the carbonyl and Michael addition to a corresponding alkene. Density Functional Theory (DFT) computations were performed to quantitatively characterize the electrophilicity of the two compounds of interest. Models of the **GDC-0810** (cinnamic acid, **A**) and **M6** (**B**) were used for this analysis (Figure 7). As **GDC-0810** and **M6** are identical aside from the respective carbonyl functionalities, the difference in reactivity can primarily be attributed to the difference in the acid and ester moieties. Thus, the truncated models provide sufficient and easy insight into the inherent reactivity. Figure 7 also displays the corresponding computed energy level of the LUMO and electrophilicity index (ω) (Parr and Szentpály, 1999; Chattaraj et al., 2006; and Domingo et al., 2016) of each model compound. As the LUMO energy is lowered, the orbital becomes more receptive towards nucleophilic addition. Additionally, ω is another measure of electrophilicity, where larger indices are indicative of stronger electrophiles (Parr and Szentpály, 1999; Chattaraj et al., 2006; and Domingo et al., 2016). As shown in Figure 7, **B** has both a lower lying LUMO and a larger electrophilicity index, indicating that it is a better electrophile than **A**. These calculated results are consistent with the experimental observations. Michael acceptors, such as the activated α,β-unsaturated ester **B**, are inherently reactive at the β-position. This inherent reactivity is also visible in the LUMO depiction of Figure 7, where the lobe of the LUMO on the β-carbon (4-position) appears visibly larger than that of the carbonyl carbon (2-position) and supports formation of GSH- or cysteine adduct products at this site. The *in silico* results quantitatively explain how acyl glucuronidation enhances the reactivity of the original α,β-unsaturated acid and therefore allows for covalent binding to proteins.

## Discussion

To investigate the mechanism of protein covalent binding of the metabolites of **GDC-0810**, several *in vitro* experiments were conducted similar to those outlined in Zhang et al (Zhang et al., 2012).

A direct conjugate of **GDC-0810** with GSH or cysteine was not observed in *in vitro* incubations, yet direct conjugates were quickly formed in incubations with **M6** to form **M13**. The fragmentation analysis of **M13**, the GSH adduct of **M6**, showed that GSH

DMD Fast Forward. Published on July 2, 2020 as DOI: 10.1124/dmd.120.000096
This article has not been copyedited and formatted. The final version may differ from this version.

added to the β-carbon, and not to the glucuronic acid moiety through a potential Schiff base (Figure 1). The Michael addition of the cysteine to **M6** was very efficient with a half-life of less than 60 min. There was no glucuronic acid replacement product by GSH or cysteine from these incubations. Direct replacement of acyl glucuronide by cysteine thiol, followed by *S*- to *N*-acyl rearrangement to form a more stable conjugate, has previously been reported (Harada et al., 2019). This produces an isomer with the same molecular ion in mass spectral analysis. We did not detect a similar displacement product during this analysis of **GDC-0810**. This is explained by the inherent reactivity differences between the compounds studied by Harada and the Michael acceptor **M6** found here. The acids in the Harada study are aliphatic or aromatic and do not contain reactive conjugated alkenes; **GDC-0810** contains an α,β-unsaturated carbonyl, which is activated by converting the acid (**GDC-0810**) to the ester (**M6**). Glutathione S-transferase (GST) catalyzed addition of GSH to electrophilic substrates is a known source of GSH conjugation to many covalent modifier drugs and reactive metabolites (Ploemen, et al, 1994; Okada et al., 2011). However, **M13** was not an identified *in vivo* metabolite in monkies. In addition, a GSH conjugate of **GDC-0810** was not formed in incubations of monkey and human liver microsomes with **GDC-0810** in the presence of GSH. Our study exemplifies how the identity of the electrophile, a Michael acceptor in this example, can dictate the reactivity with biologically active thiols. Quantum mechanical calculations were able to quantify the inherent reactivity differences between α,β-unsaturated functional groups, and illustrates how computations can complement our understanding to better predict the susceptibility of electrophilic moieties to nucleophiles such as GSH. This should be considered when elucidating the metabolic profile of compounds.

The **GDC-0810** scaffold contains two extensively conjugated alkene moieties generally considered to be susceptible to CYP-mediated epoxidation, forming reactive intermediates. These reactive intermediates could be susceptible to further reaction such as hydrolytic ring opening and alkylation. We were intrigued to find that, after incubation with human or monkey liver microsomes, no oxidative metabolites of **GDC-0810** (M+16) were detected. Additionally, when **M4**, **M6**, and **GDC-0810** were incubated with liver microsomes fortified with NADPH and GSH, GSH conjugation to oxidized

DMD Fast Forward. Published on July 2, 2020 as DOI: 10.1124/dmd.120.000096
This article has not been copyedited and formatted. The final version may differ from this version.

metabolites (M+323) was not observed. **M3**, an oxidative metabolite of the di-glucuronide **M1**, was a prominent circulating metabolite in monkey *in vivo*, along with **M6**, but the potential reactivity of **M3** could not be assessed due to lack of a metabolite standard. These results suggest the potential for CYP-mediated bioactivation for **GDC-0810** is very low in monkeys or humans. Acyl glucuronidation of gemfibrozil and clopidogrel led to CYP 2C8-mediated bioactivation. This resulted in significant clinical drug-drug interactions with those drugs metabolized by CYP 2C8 (Ma et al., 2017; Ogilvie et al., 2006; Itkonen et al., 2019). CYP inactivation was not reported in the case of **GDC-0810**. It should also be mentioned that toxicity findings associated with **GDC-0810** bioactivation have not been reported.

From the incubations in liver microsomes fortified with NADPH and GSH, we, instead, observed the GSH conjugate of glucuronide metabolite **M13** (M+307 of **M6**). This is consistent with the previous experiment in buffer incubations with **M6**. These observations suggest that **GDC-0810** is explicitly bioactivated via glucuronidation. No GSH adducts were identified from the trapping incubations with **GDC-0810** or **M4**.

The mechanism of bioactivation discussed within this manuscript is distinct from previously reported examples. Carboxylic acid-containing compounds can form acyl coenzyme A (CoA) conjugates through acyl adenylate intermediate (adenosine monophosphate, AMP). The acyl CoA conjugates can be more reactive than the corresponding acyl glucuronides and can further react to form glycine or taurine conjugates (Lassila et al., 2015; Grillo et al., 2003; Grillo et al., 2012; Darnel et al, 2015; Lassila et al, 2015). Here, no acyl adenylate intermediate metabolites were observed in incubations of **GDC-0810** in hepatocytes. While the Michael addition of a thiol to the acyl glucuronide of GDC-0810 was efficient, which can explain its protein binding potential, the possibility of forming acyl CoA thioester conjugates as a contributing factor of covalent binding of GDC-0810 cannot be ruled out. Identification of in vitro acyl CoA conjugates would be complicated by rapid degradation in the hepatocyte incubations, and our in vitro methods were not optimized for detection.

Another covalent binding mechanism appeared to correlate, in general, with the chemical stability of the acyl glucuronides (Zhong et al., 2015; Sawamura et al., 2010;

DMD Fast Forward. Published on July 2, 2020 as DOI: 10.1124/dmd.120.000096
This article has not been copyedited and formatted. The final version may differ from this version.

Zhang et al., 2011). **M6** is very stable in buffer with a half-life of greater than eight hours. In comparison, diclofenac acyl glucuronide has a half-life of less than one hour under similar conditions (Zhang et al., 2011). This incredible stability indicates that while **M6** is converted to a great electrophile for protein conjugation, it is not activated to undergo degredation or other metabolic processes. Bioactivation by glucuronidation has only been previously described to result in transacylation or glycation via Amadori rearrangement (Skonberg et al., 2008; Miyashita et al., 2014; Ding et al., 1993; Harada et al., 2019). No GSH addition to the glucuronic acid moiety was observed, even though acyl migration isomers were detected in these *in vitro* incubations. Collectively, our results suggested that bioactivation of α,β-unsaturated acids was via glucuronidation and thus led to its covalent binding to proteins via Michael addition. Acyl glucuronidation of GDC-0810 increased the inherent reactivity, making the β-position of the double bond more reactive toward nucleophiles.

Tandem bioactivation-protein conjugation with the acyl glucuronidation of α,β-unsaturated acids represents a novel bioactivitation mechanism. There are limited examples that demonstrate the chemical modifications which occur after non-P450 mediated or P450-mediated bioactivation and the impact on covalent binding to proteins (Gan et al., 2016). Covalent binding of acetaminophen to proteins occurs through conjugation of a cysteine thiol to its quinone imine intermediate (Leeming et al., 2015). MaxiPost is reported to form irreversible covalent binding with plasma proteins, mostly serum albumins, in humans, dogs, and rats, through Michael addition of the ***ε***-amino group of an albumin lysine to a proposed quinone methide intermediate (Zhang et al., 2005). A number of covalent inhibitors (e.g. neratinib, osimertinib, and ibrutinib) also have shown certain degrees of endogenous protein adduct formation. Neratinib was found to form covalent adducts on Lys-190 of human serum albumin, but did not react to the free thiol of cysteine in albumin (Wang et al., 2010). **GDC-0810** was quantitatively recovered from 24 h incubations in human or monkey plasma, supporting that there was no direct reaction between the compound and plasma proteins. Our study demonstrates a new mode of tandem bioactivation-protein conjugation with the acyl glucuronidation of **GDC-0810**. It is interesting to note that AZD9496, also a target protein degrader, contains an α,β-unsaturated carboxylic acid as well (Puyang, et al., 2018; Savi et al.,

DMD Fast Forward. Published on July 2, 2020 as DOI: 10.1124/dmd.120.000096
This article has not been copyedited and formatted. The final version may differ from this version.

2015). Given our studies within this paper, one would expect that a similar bioactivation-protein conjugation pathway is feasible for this candidate. Several reports of α,β-unsaturated carboxylic acid glucuronide metabolites exist in literature, but none mention Michael addition reactions as a possible bioactivation mechanism. Primary considerations of these reports on the risk of covalent binding were associated with acyl glucuronide rearrangements (Kenny et al., 2005; Kaul and Olson, 1998; Sass et al., 1995; Nakazawa et al., 2010; Piazzon et al., 2012).

α,β-Unsaturated amides are excellent Michael acceptors and a number of covalent inhibitor drugs (e.g. neratinib, osimertinib, and ibrutinib) are designed with acrylamide moieties to react with free thiols of cysteine residues in target proteins. α,β-Unsaturated esters have also been explored as a potential warheads to react with a free thiols in target proteins (Gehringer and Laufer et al., 2019). It is not known if **M6** could covalently bind to ERα protein, leading to degradation of the target. Additional studies would be needed to evaluate if an α,β-unsaturated carboxylic acid can serve as the prodrug strategy, utilizing our identified bioactivation mechanism, to activate a compound for covalent binding to the target receptor.

In summary, acyl glucuronidation of the α,β-unsaturated carboxylic acid in **GDC-0810** activates the conjugated alkene towards nucleophilic addition by GSH or other reactive thiols. This is the first example of bioactivation of α,β-unsaturated carboxylic acid compounds leading to covalent binding to proteins.

**Acknowledgements**

The authors thank Dian Su, Tom De Bruyn, Jun Liang and Gina Wang from Genentech for review of the manuscript. All authors are Genentech employees when the research was conducted.

Authorship Contributions

Participated in research design: Zhang D, Mulder, Khojasteh

DMD Fast Forward. Published on July 2, 2020 as DOI: 10.1124/dmd.120.000096
This article has not been copyedited and formatted. The final version may differ from this version.

Conduct experiments: Mulder, Bobba, Johnson, Wang, Zhang C, Cai

Contributed new reagents or analytic tools:

Performed data analysis: Mulder, Bobba, Johnson, Grandner, Wang, Zhang C, Cai, Choo, Khojasteh, Zhang D

Wrote or contributed to writing of the manuscript: Zhang D, Mulder, Johnson, Grandner, Khojasteh

DMD Fast Forward. Published on July 2, 2020 as DOI: 10.1124/dmd.120.000096
This article has not been copyedited and formatted. The final version may differ from this version.

## References

Jemal, A., Bray, F., Center, M. M., Ferlay, J., Ward, E., and Forman, D. (2011) Global cancer statistics. *C.A. Cancer J. Clin*. 61, 69–90.

Barone, V.; Cossi, M. (1988) Quantum Calculation of Molecular Energies and Energy Gradients in Solution by a Conductor Solvent Model. *J. Phys. Chem. A*, 102, 1995-2001.

Baselga, J., Campone, M., Piccart, M., Burris III, H.A., Rugo, H.S., Sahmoud, T., Noguchi, S., Gnant, M., Pritchard, K.I., Lebrun, F. and Beck, J.T. (2012) Everolimus in Postmenopausal Hormone-Receptor–Positive Advanced Breast Cancer. *N. Engl. J. Med*. 366, 520–529.

Chattaraj, P. K.; Sarkar, U.; Roy, D. R. (2006) Electrophilicity Index. *Chem. Rev.* 106, 6, 2065-2091.

Cossi, M.; Rega, N.; Scalmani, G.; Barone, V. (2003) Energies, structures, and electronic properties of molecules in solution with the C-PCM solvation model. *J. Comp. Chem.*24, 669-681.

Darnel, M., Breitholtz, K., Isin, E.M., Jurva, U., and Weidolf, L. (2015) Significantly Different Covalent Binding of Oxidative Metabolites, Acyl Glucuronides, and S-Acyl CoA Conjugates Formed from Xenobiotic Carboxylic Acids in Human Liver Microsomes *Chem. Res. Toxicol*. 28, 886-896.

Di Leo, A., Jerusalem, G., Petruzelka, L., Torres, R., Bondarenko, I. N., Khasanov, R. Verhoeven, D.,Pedrini, J.L., Smirnova, I., Lichinitser, M.R., Pendergrass, K., Garnett, S.,Lindemann, J.P., Sapunar, F., and Martin, M. (2010) Results of the CONFIRM phase III trial comparing fulvestrant 250 mg with fulvestrant 500 mg in postmenopausal women with estrogen receptor-positive advanced breast cancer. *J. Clin. Oncol*. 28, 4594–4600.

Ding, A., Ojingwa, J.C., McDonagh, A.F., Burlingame, A.L., Benet, L.Z. (1993) Evidence for covalent binding of acyl glucuronides to serum albumin via an imine mechanism as revealed by tandem mass spectrometry. *Proc. Natl. Acad. Sci*. 90, 3797-801.

Domingo, L. R.; Ríos-Gutiérrez, M; Pérez, P. (2016) Applications of the Conceptual Density Functional Theory Indices to Organic Chemistry Reactivity. *Molecules*, 21, 748.

Gan, J., Ma, S., Zhang, D. (2016) Non-P450 mediated drug bioactivation pathways and its toxicological relevance. *Drug Metab. Rev*. 48, 473-501.

Gehringer M and Laufer SA (2019) Emerging and Re-Emerging Warheads for Targeted Covalent Inhibitors: Applications in Medicinal Chemistry and Chemical Biology. *J. Med. Chem*, 62, 5673-5724.

Grillo, M. P., Hua, F., Knutson, C. G., Ware, J. A., Li, C. (2003) Mechanistic studies on the bioactivation of diclofenac: Identification of diclofenac-S-acyl-glutathione in vitro in incubations with rat and human hepatocytes *Chem. Res. Toxicol*. 16, 1410– 1417.

Grillo, M. P., Lohr, M. T., and Wait, J. C. M. (2012) Metabolic activation of mefenamic acid leading to mefenamyl-S-acyl-glutathione adduct formation in vitro an in vivo in rat *Drug Metab. Dispos*. 40, 1515– 1526.

Halgren, T. A. (1996a) Merck molecular force field. I. Basis, form, scope, parameterization, and performance of MMFF94. *J. Comp. Chem.* 17, 490-519.

Halgren, T. A. (1996b) Merck molecular force field. II. MMFF94 van der Waals and electrostatic parameters for intermolecular interactions. *J. Comp. Chem.* 17, 520-552.

Halgren, T. A. (1996c) Merck molecular force field. III. Molecular geometries and vibrational frequencies for MMFF94. *J. Comp. Chem.* 17, 553-586.

Halgren, T. A. (1996d) Merck molecular force field. V. Extension of MMFF94 using experimental data, additional computational data, and empirical rules. *J. Comp. Chem.* 17, 616-641

Halgren, T. A.; Nachbar, R. B. (1996) Merck molecular force field. IV. conformational energies and geometries for MMFF94. *J. Comp. Chem.* 17, 587-615.

Harada, H., Toyoda, Y., Abe, Y., Endo, T., and Takeda, H. (2019) Quantitative Evaluation of Reactivity and Toxicity of Acyl Glucuronides by [$^{35}$S]Cysteine Trapping. *Chem. Res. Toxicol*. 32, 1955-1964.

Hop, C. E. C. A., Wang, Z., Chen, Q., & Kwei, G. (1998). Plasma-pooling methods to increase throughput for in vivo pharmacokinetic screening. *J. Pharm. Sci.* 87, 901–903.

Itkonen, M.K., Tornio, A., Neuvonen, M., Neuvonen, P.J., Niemi, M. and Backman, J.T. (2019) Clopidogrel and Gemfibrozil Inhibit Desloratadine Metabolism. *Drug Metab. Dispos.* 47, 377-385.

Jemal, A., Bray, F., Center, M. M., Ferlay, J., Ward, E., and Forman, D. (2011) Global cancer statistics. *C.A. Cancer J. Clin*. 61, 69–90.

Kaul, S., & Olson, J. A. (1998) Effect of vitamin A deficiency on the hydrolysis of retinoyl beta-glucuronide to retinoic acid by rat tissue organelles in vitro. *Int J Vitam Nutr Res*, 68, 232-236.

Kenny, J. R., Maggs, J. L., Tettey, J. N., Harrell, A. W., Parker, S. G., Clarke, S. E., & Park, B. K. (2005) Formation and protein binding of the acyl glucuronide of a leukotriene B4

antagonist (SB-209247): relation to species differences in hepatotoxicity. *Drug Metab. Dispos*. 33, 271–281.

Lassila,T., Hokkanen, J., Aatsinki, S.-M., Mattila,S., Turpeinen, M., and Tolonen, A. (2015) Toxicity of Carboxylic Acid-Containing Drugs: The Role of Acyl Migration and CoA Conjugation Investigated. *Chem Res. Toxicol.* 28, 2292-2303.

Leeming, M.G., Gamon, L.F., Wille, U., Donald, W.A., O'Hair, R.A. (2015) What Are the Potential Sites of Protein Arylation by N-Acetyl-p-benzoquinone Imine (NAPQI)? *Chem Res. Toxicol*. 28, 2224–2233.

Ma, Y., Chen, Y., Khojasteh, S.C., Dalvie, K., Zhang, D. (2017) Glucuronides as anionic substrates of human CYP2C8. *J. Med. Chem*. 60, 8691-8705.

Miyashita, T., Kimura, K., Fukami, T., Nakajima, M., Yokoi, T. (2014) Evaluation and mechanistic analysis of the cytotoxicity of the acyl glucuronide of nonsteroidal antiinflammatory drugs. *Drug Metab. Dispos*. 42, 1-8.

Miller, T. W., Hennessy, B. T., González-Angulo, A. M., Fox, E. M., Mills, G. B., Chen, H., Higham C., García-Echeverría C., Shyr Y., Arteaga, C. L. (2010) Hyperactivation of phosphatidylinositol-3 kinase promotes escape from hormone dependence in estrogen receptor-positive human breast cancer. *J. Clin. Invest*. 120, 2406–2413.

Nakazawa, T., Yasuda, T., and Ohsawa, K. (2010) Metabolites of orally administered Magnolia officinalis extract in rats and man and its antidepressant-like effects in mice. *J. P. P.* 55, 1583–1591.

Ogilvie, B.W., Zhang, D., Li, W., Rodrigues, A.D., Gipson, A.E., Holsapple, J., Toren, P., and Parkinson, A. (2006) Glucuronidation converts gemfibrozil to a potent, metabolismdependent inhibitor of CYP2C8: implications for drug-drug interactions. *Drug Metab. Dispos.* 34: 191-197.

Okada, R., Maeda, K., Nishiyama, T., Aoyama, S., Tozuka, Z., Hiratsuka, A., Ikeda, T., Kusuhara, H., and Sugiyama, Y. (2011) Involvement of Different Human Glutathione Transferase Isoforms in the Glutathione Conjugation of Reactive Metabolites of Troglitazone. *Drug Metab. Dispos*. 39, 2290-2297.

Parr, R. G.; Szentpály, L. v.; Liu, S. (1999) Electrophilicity Index. *J. Am. Chem. Soc.* 121, 1922-1924.

Piazzon, A., Vrhovsek, U., Masuero, D., Mattivi, F., Mandoj, F., and Nardini, M. Antioxidant (2012) Activity of Phenolic Acids and Their Metabolites: Synthesis and Antioxidant Properties of the Sulfate Derivatives of Ferulic and Caffeic Acids and of the Acyl Glucuronide of Ferulic Acid. *J. Agric. Food Chem*. 60, 12312-12323.

Ploemen, J.H.T.M., Van Schanke, Z.A., Van Ommen B., and Van Bladeren P.J. (1994) Reversible Conjugation of Ethacrynic Acid with Glutathione and Human Glutathione S-Transferase PI-1. *Cancer Res.* 54, 915-919.

Puyang X, Furman C, Zheng GZ, Wu ZJ, Banka D, Aithal B K, Agoulnik S, Bolduc DM, Buonamici S, Caleb B, Das S, Eckley S, Fekkes P, Hao MH, Hart A, Houtman R, Irwin S, Joshi JJ, Karr C, Kim A, Kumar N, Kumar P, Kuznetsov G, Lai WG, Larsen N, MacKenzie C, Martin LM, Melchers D, Moriarty A, Nguyen TV, Norris J, O'Shea M, Pancholi S, Prajapati S, Rajagopalan S, Reynolds DJ, Rimkunas V, Rioux N, Ribas R, Siu A, Sivakumar S, Subramanian V, Thomas M, Vaillancourt FH, Wang J, Wardell S, Wick MJ, Yao S, Yu L, Warmuth M, Smith PG, Zhu P and Korpal M (2018) Discovery of Selective Estrogen Receptor Covalent Antagonists (SERCAs) for the treatment of ERa(WT) and ERa(MUT) breast cancer. *Cancer Discov*, 8: 1176-1193.

Roothaan, C. C. J. (1951) New Developments in Molecular Orbital Theory. *Rev. Mod. Phys.* 23, 69.

Metabolism of oral 9-cis-retinoic acid in the human. Identification of 9-cis-retinoyl-beta-glucuronide and 9-cis-4-oxo-retinoyl-beta-glucuronide as urinary metabolites. *Drug Metab. Dispos*. 23, 887-891.

Savi CD, Bradbury RH, Rabow AA, Norman RA, de Almeida C, Andrews DM, Ballard P, Buttar D, Callis RJ, Currie GS, Curwen JO, Dvies CD, Donald CS, Feron LJL, Gingell H, Glossop SC, Hayter BR, Hussain S, Karoutchi G, Lamont SG, MacFaul P, Moss TA, Pearson SE, Tonge M, Walker GE, and Weir HM (2015) Optimization of a novel binding motif to (E)-3-(3,5-Difluoro-4-((1R,3R)-2-(2-fluoro-2-methylpropyl)-3-methyl-2,3,4,9tetrahydro-1H-pyrido[3,4-b]indol-1-yl)phenyl)acrylic acid (AZD9496), a potent and orally bioavailable selective estrogen receptor downregulator and antagonist. *J. Med. Chem.* 58: 8128-8140.

Sawamura, R., Okudaira, N., Watanabe, K., Murai, T., Kobayashi, Y., Tachibana, M., Ohnuki,T., Masuda, K., Honma, H., Kurihara, A., Okazaki, O. (2010) Predictability of Idiosyncratic Drug Toxicity Risk for Carboxylic Acid-containing Drugs Based on the Chemical Stability of Acyl Glucuronide. *Drug Metab. Dispos.* 38, 1857–1864.

Skonberg, C., Olsen, J., Madsen, K.G., Hansen, S.H., Grillo, M.P. (2008) Metabolic activation of carboxylic acids. *Expert Opin. Drug Metab. Toxicol.* 4, 425-438.

Van Tine, B., Crowder, R., Ellis, M. (2012) ER and PI3K independently modulate endocrine resistance in ER positive breast cancer. *Cancer Discov*. 1, 287–288.

Wang J, Li-Chan XX, Atherton J, Deng L, Espina R, Yu L, Horwatt P, Ross S, Lockhead S,

Ahmad S, Chandrasekaran A, Oganesian A, Scatina J, Mutlib A, and Talaat R (2010) Characterization of HKI-272 covalent binding to human serum albumin. *Drug Metab Dispos* 38:1083–1093.

Y.Shao et al. (2015) Advances in molecular quantum chemistry contained in the Q-Chem 4 program package. *Mol. Phys.* 113, 184-215.

Zhang, D., Krishna, R., Wang, L., Zeng, J., Mitroka, J., Dai, R., Narasimhan, N., Reeves, R.A., Srinivas, S.R., and Klunk, L.J. (2005) Metabolism, pharmacokinetics, and protein covalent binding of C-14 labeled Maxipost in humans. *Drug Metab. Dispos*. 33, 83-93.

Zhang, D., Luo, G., Ding, X., Lu, C. (2012) Preclinical Experimental Models of Drug Metabolism and Disposition in Drug Discovery and Development. *Acta Pharm. Sin. B.* 2, 549-561.

Zhang, D., Raghavan, N., Wang, L., Xue, Y., Obermeier, M., Chen, S., Tao, S., Zhang, H., Cheng, P.T., Li, W., Ramanathan, R., Yang, Z. and Humphreys, W.G. (2011) Plasma Stability-Dependent Circulation of Acyl Glucuronide Metabolites in Humans: How Circulating Metabolite Profiles of Muraglitazar and Peliglitazar Can Lead to Misleading Risk Assessment. *Drug Metab. Dispos.* 39, 123-131.

Zhao, Y.; Truhlar. D. G. (2008) The M06 suite of density functionals for main group thermochemistry, thermochemical kinetics, noncovalent interactions, excited states, and transition elements: two new functionals and systematic testing of four M06-class functionals and 12 other functionals. *Theor. Chem. Acc.* 120, 215-241.

Zhong, S., Jones, R., Lu, W., Schadt, S., and Ottaviani, G. (2015) A New Rapid in vitro Assay for Assessing Reactivity of Acyl Glucuronides. *Drug Metab. Dispos.* 43, 1711–1717.

DMD Fast Forward. Published on July 2, 2020 as DOI: 10.1124/dmd.120.000096
This article has not been copyedited and formatted. The final version may differ from this version.

**List of Figures:**

DMD Fast Forward. Published on July 2, 2020 as DOI: 10.1124/dmd.120.000096
This article has not been copyedited and formatted. The final version may differ from this version.

**Table 1 Exposure of Radioactivity (ng/g equivalent of [$^{14}$C]GDC-0810) of [$^{14}$C]GDC-0810 and Its Identified Metabolites in Pooled Plasma Samples from Intact Female Monkeys Following a Single Oral Dose of 50 mg/kg**

| Analyte | Exposure (ng/g equivalent) per time-point (hour) | | | | | |
|---|---|---|---|---|---|---|
| | 3 | 6 | 12 | 24 | 48 | 72 |
| GDC-0810 | 1151 | 3332 | 339 | 179 | 22 | 16 |
| M1 [c] | D | D | D | D | ND | ND |
| M3 | D | 32 | 515 | 56 | 22 | 32 |
| M5 [a] | D | D | 176 [b] | D | D | ND |
| M11 [a] | D | D | | D | ND | ND |
| M6 | 2303 | 4794 | 176 | 100 | 76 | 32 |
| M7 | D | D | D | D | D | ND |
| ng equivalents/g characterized | 3454 | 9206 | 1206 | 335 | 120 | 80 |
| ng equivalents/g in sample | 4860 | 12900 | 2840 | 806 | 515 | 380 |
| Sample Extraction Recovery (%) | 82 | 75.9 | 51.9 | 45.7 | 38 | 25.4 |

ND = not detected; D = detected only by mass spectrometry.

Note: Metabolites were numbered according to retention time except for parent compound (**GDC-0810**).

[a] M5 co-eluted with **M11** in plasma. [b] Value represents total of M5 and **M11**.

[c] M1 was a di-glucuronide and M3 was oxidative di-glucuronide (see supplemental Fig S1).

**Table 2 Molecular Ion and Major Product Ions Observed for GDC-0810 and Its Metabolites**

| Analyte | RT [a] (min) | Observed $[M + H]^+$ (*m/z*) | Theoretical $[M + H]^+$ (*m/z*) | Mass Accuracy (ppm) | Chemical Formula | Matrix [b] | Major Fragment Ions (*m/z*) |
|---|---|---|---|---|---|---|---|
| GDC-0810 | 45.96 | 447.1270 | 447.1270 | 0.0 | $C_{26}H_{21}ClFN_2O_2^+$ | p , u, b, f | 429.1179, 299.0759, 284.0523, 263.0992, 311.0647, 169.0764, 143.0060 |
| M1[d] | 17.29 | 799.1917 | 799.1912 | -0.6 | $C_{38}H_{37}ClFN_2O_{14}^+$ | p, u | 623.1625, 447.1294, 299.0770 |
| M3[d] | 17.84 | 815.1860 | 815.1861 | 0.1 | $C_{38}H_{37}ClFN_2O_{15}^+$ | p, u, b | 797.1779, 639.1554, 621.1442, 463.1226, 445.1122, 315.0706, 309.0478 |
| M4 | 19.63 | 623.1592 | 623.1591 | -0.2 | $C_{32}H_{29}ClFN_2O_8^+$ | p, u, b | 605.1494, 447.1287, 311.0655, 299.0760 |
| M5 | 17.14 | 639.1541 | 639.1540 | -0.2 | $C_{32}H_{29}ClFN_2O_9^+$ | p | 505.1396, 463.1237, 446.1181, 315.0710, 309.0478 |
| M6 | 30.86 | 623.1590 | 623.1591 | 0.2 | $C_{32}H_{29}ClFN_2O_8^+$ | p, u, b | 605.1500, 447.1286, 311.0645, 299.0759, 263.0961 |
| M7 | 39.17 | 463.1216 | 463.1219 | 0.6 | $C_{26}H_{21}ClFN_2O_3^+$ | b | 446.1206, 411.1521, 315.0708, 311.0648, 185.0713, 143.0059 |
| M11 | 18.29 | 744.1790 | 744.1788 | -0.3 | $C_{35}H_{36}ClFN_3O_{10}S^+$ | p, u, b | 726.1737, 623.1620, 568.1501, 447.1300, 403.1398 |
| M13 | 7.11 | 465.6254[c] | 465.6251 | -0.6 | $C_{27}H_{29}F_3N_5O_8^+$ | In vitro | 447.1266, 405.1169, 299.0750, 203.0624, 162.0220, 130.0501 |
| M14 | 7.48 | 377.6089[c] | 377.6090 | 0.3 | $C_{36}H_{38}ClFN_5O_8S^+$ | In vitro | 447.1272, 405.1167, 340.0946, 299.0743, 203.0624, 162.0217, 130.0501, 84.0449 |

$[M + H]^+$ = protonated molecular ion; min = minutes; *m/z* = mass-to-charge ratio; p = plasma; u = urine; b = bile; f = feces; ppm = parts per million; RT = retention time (min); [a] LC-MS retention times are from metabolite profiling of matrix that has the most abundant metabolites. Some retention time shift was observed for different matrices; [b] Sample matrix showing radioactive peak (excluding buffer); [c] Z=2 doubly charged; [d] M1 was a di-glucuronide and M3 was oxidative di-glucuronide.

DMD Fast Forward. Published on July 2, 2020 as DOI: 10.1124/dmd.120.000096
This article has not been copyedited and formatted. The final version may differ from this version.

Figure 1

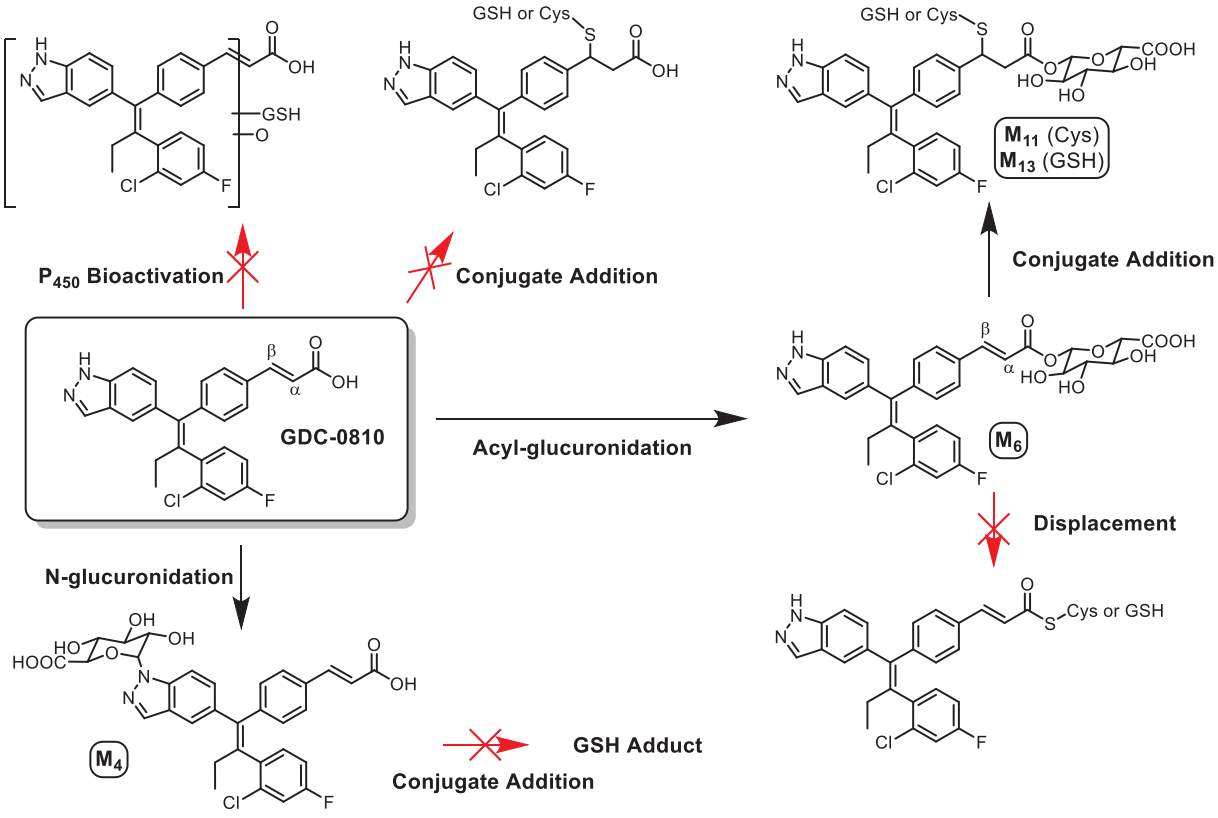

DMD Fast Forward. Published on July 2, 2020 as DOI: 10.1124/dmd.120.000096
This article has not been copyedited and formatted. The final version may differ from this version.

Figure 2

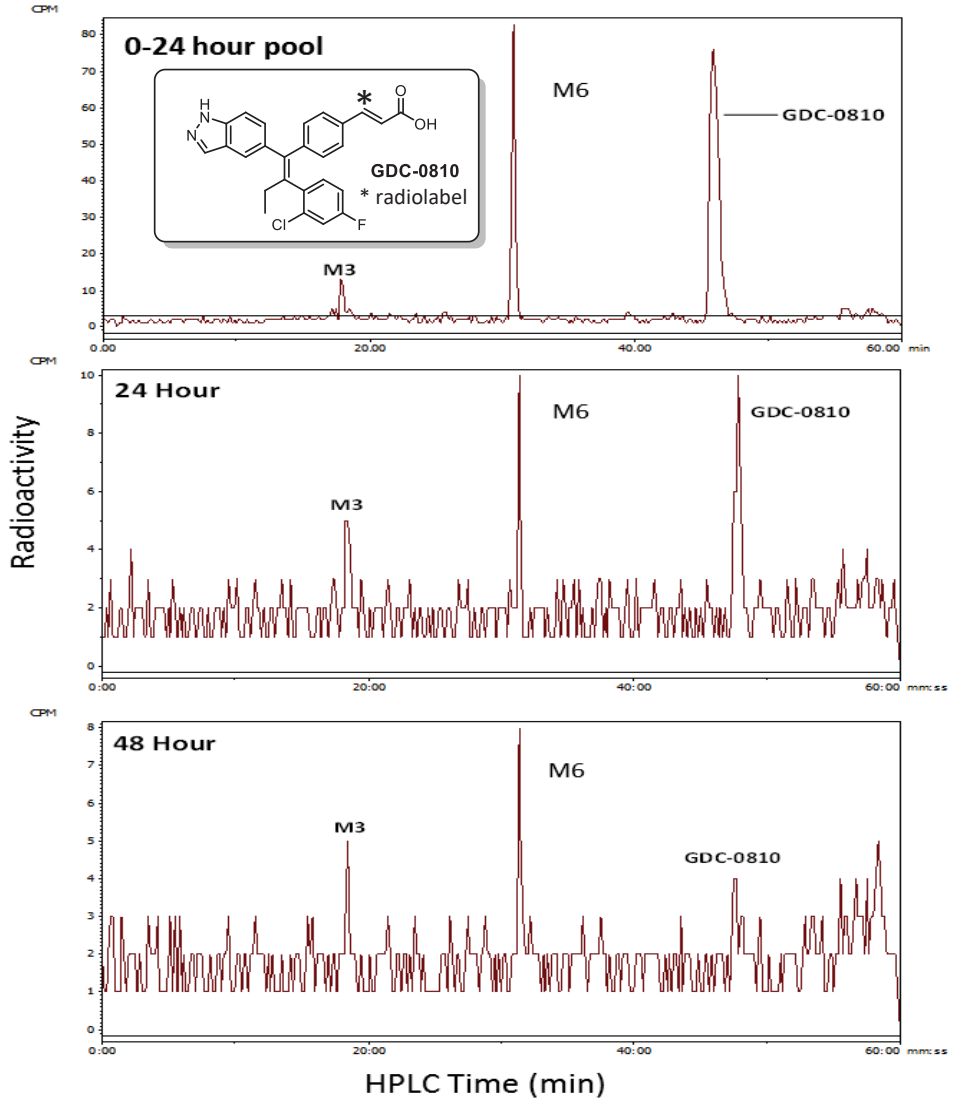

DMD Fast Forward. Published on July 2, 2020 as DOI: 10.1124/dmd.120.000096
This article has not been copyedited and formatted. The final version may differ from this version.

Figure 3

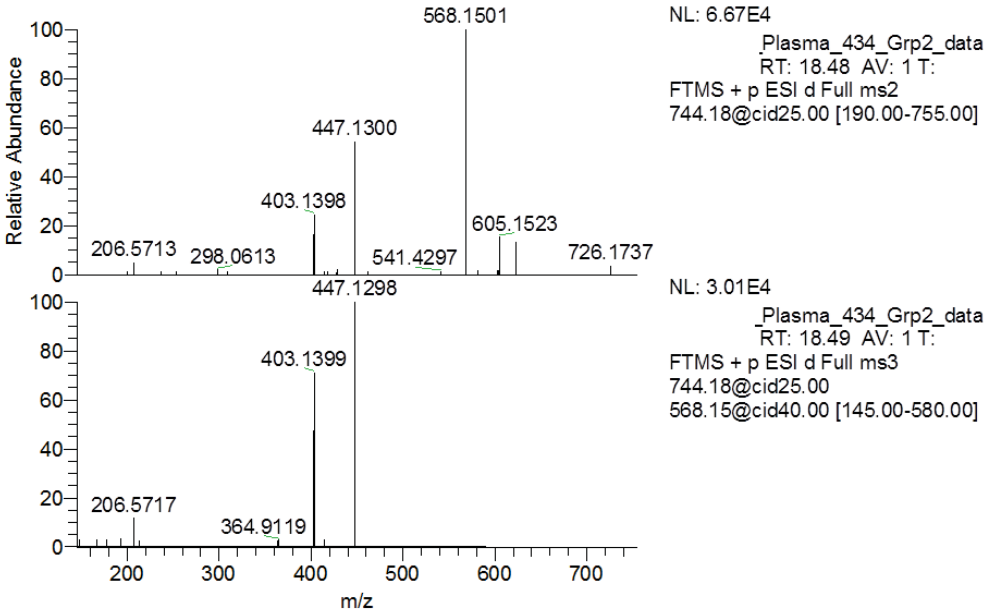


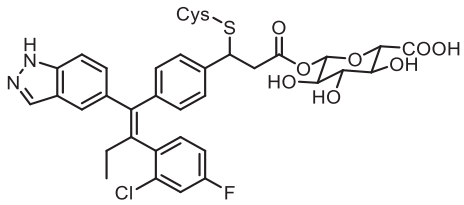


$[M+H]^+ = 744$
744 - $H_2O$ = 726
744 - Cys - H= 623
744 - Gluc = 568
744 - Gluc -Cys -H = 447
447 - COOH +H = 403

ESI = electrospray ionization; cid = collision-induced dissociation; F = scan filter; FTMS = Fourier transform mass spectrometry; m/z = mass-to-charge ratio; MS/MS = tandem mass spectrometry; NL = normalized level to the average base peak; RT = retention time (min).

DMD Fast Forward. Published on July 2, 2020 as DOI: 10.1124/dmd.120.000096
This article has not been copyedited and formatted. The final version may differ from this version.

Figure 4

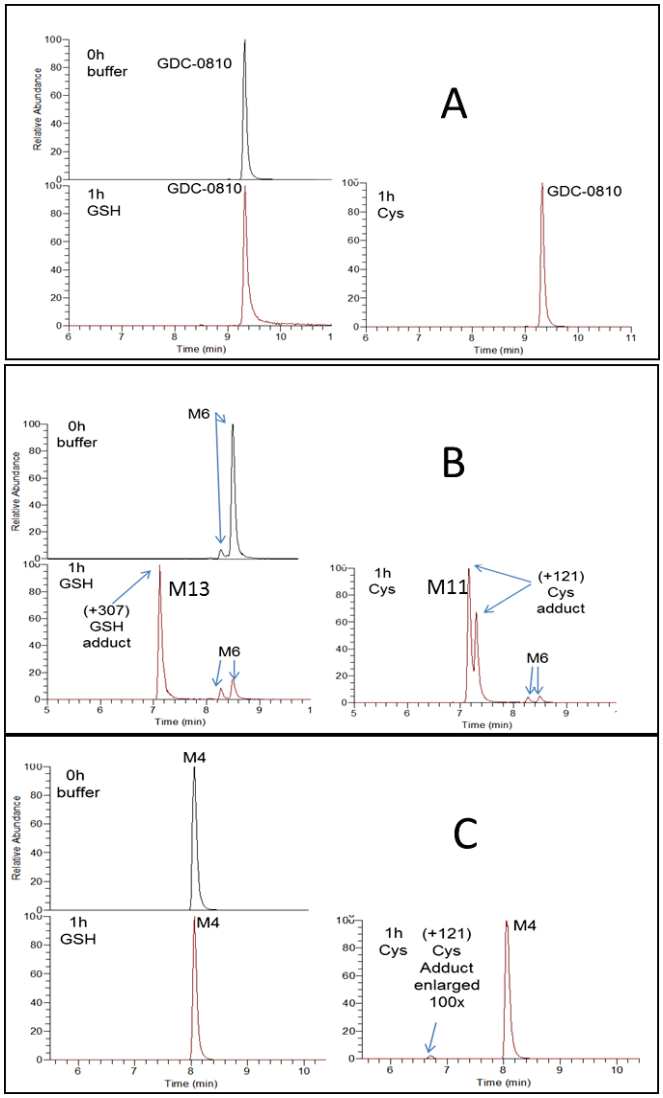

DMD Fast Forward. Published on July 2, 2020 as DOI: 10.1124/dmd.120.000096
This article has not been copyedited and formatted. The final version may differ from this version.

Figure 5

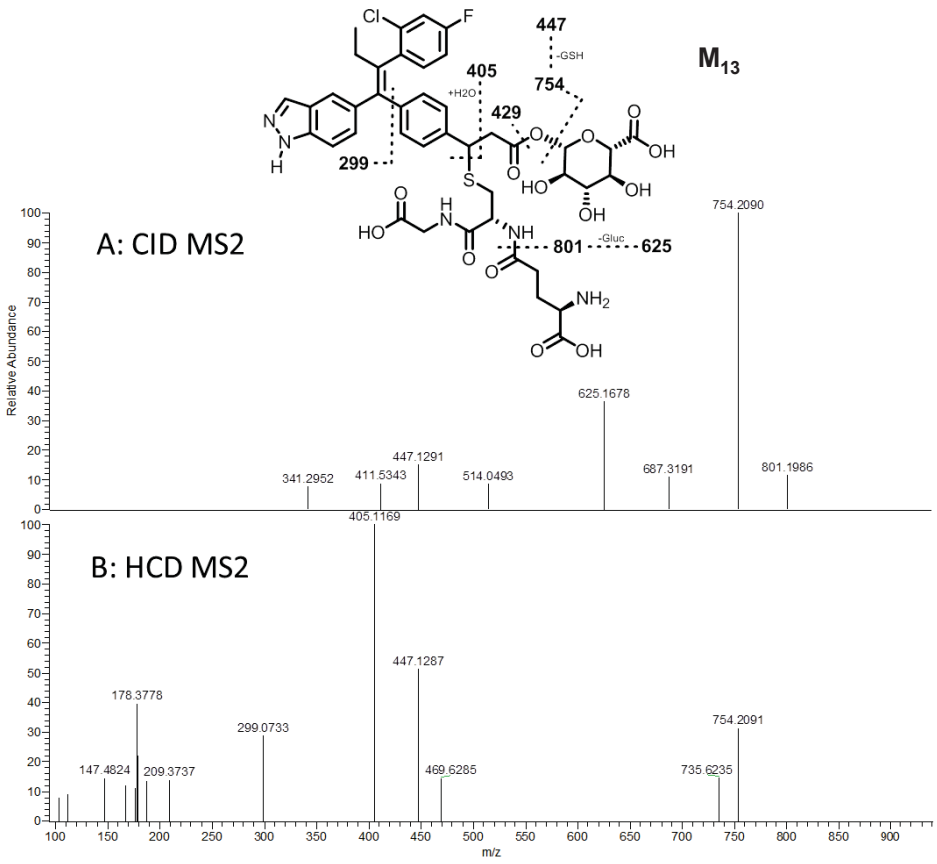

DMD Fast Forward. Published on July 2, 2020 as DOI: 10.1124/dmd.120.000096
This article has not been copyedited and formatted. The final version may differ from this version.

Figure 6

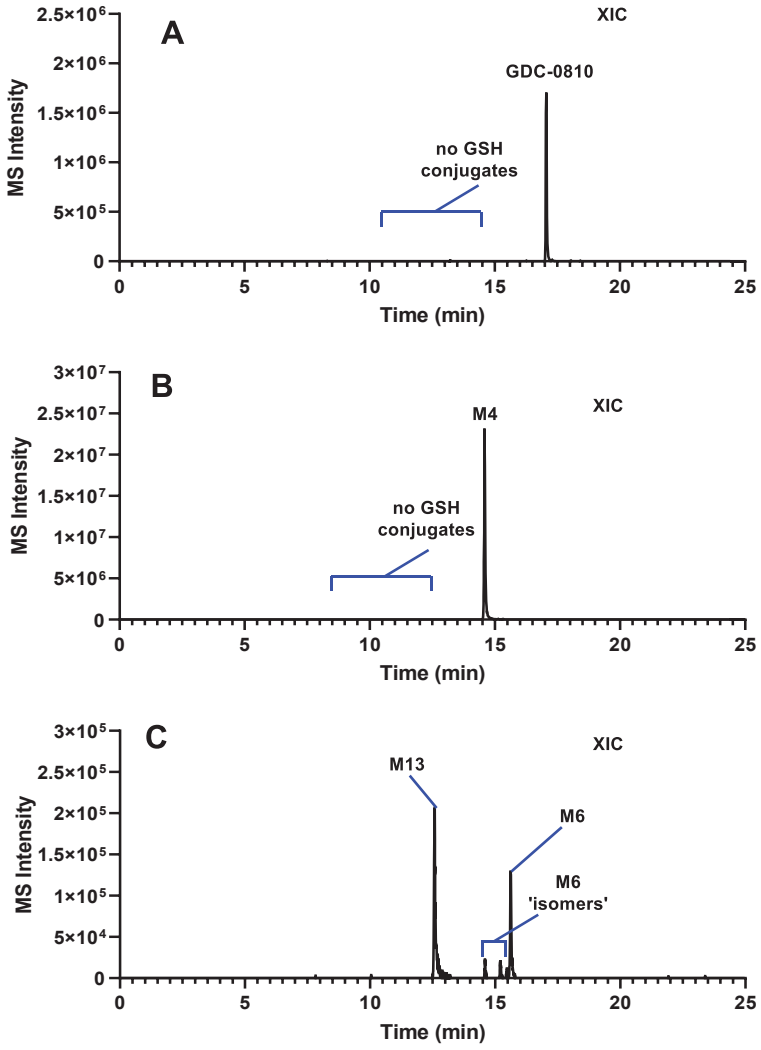

DMD Fast Forward. Published on July 2, 2020 as DOI: 10.1124/dmd.120.000096
This article has not been copyedited and formatted. The final version may differ from this version.

Figure 7

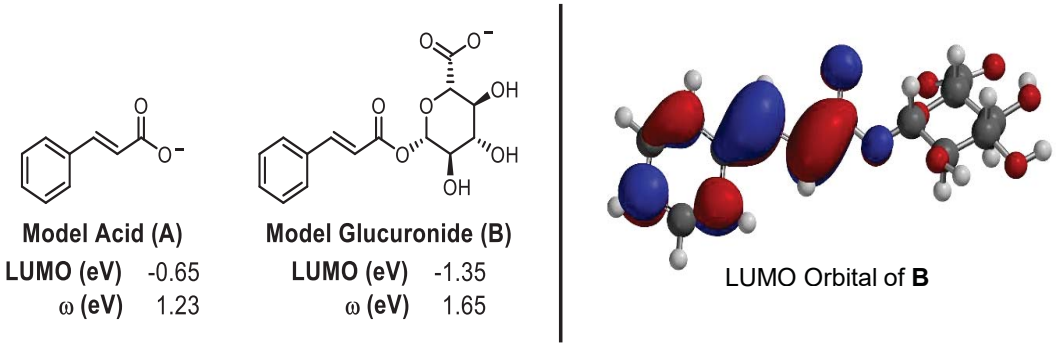

**Supplemental Information**

# Bioactivation of α,β-Unsaturated Carboxylic Acids Through Acyl Glucuronidation

Teresa Mulder, Sudder Bobba, Kevin M. Johnson, Jessica M. Grandner, Wei Wang, Chenghong Zhang, Jingwei Cai, Edna F. Choo, S. Cyrus Khojasteh, Donglu Zhang

**Monkey plasma collection, extraction, and profiling**

Groups 1 and 2 consisted of three intact and three bile duct-cannulated (BDC) female monkeys respectively. Animals were orally dosed at 50 mg/kg. Blood samples containing 40 mM citric acid were collected from animals in Group 1 (intact) and Group 2 (BDC) at predose; at 0.25, 0.5, 1, 3, 6, 9, 12, 24, 48, and 72 hours post-dose. Urine was collected from animals in Groups 1 and 2 at approximately predose; 0–8 and 8–24 hours post-dose; and at 24-hour intervals up to 168 hours post-dose. Bile was collected from BDC monkeys (Group 2) at predose; 0–3, 3–8, and 8–24 hours post-dose; and at 24-hour intervals up to 168 hours post-dose. Urine and bile samples were acidified with citric acid for the final concentration around 60 mM. Fecal samples were collected from animals in Groups 1 and 2 at approximately 12-hour intervals through 168 hours post-dose. Feces samples were homogenized on wet ice in approximately three volumes (w/v) of 80 mM citric acid in water:ethanol (1:1, v:v).

Monkey plasma samples at 0.25, 0.5, 1, 3, 6, 9, 12, and 24 hours post-dose were pooled accordingly to produce $AUC_{0\text{-}24h}$ samples. Each subject was pooled as separate samples. Individual time points of 1, 3, 6, 12, 24, 48, and 72 hours post-dose were pooled by equal volume of sample to produce two sets of samples per time point (intact and BDC).[31]

Plasma sample was combined with 3x volume of 0.1% formic acid in acetonitrile. The samples were mixed by vortex for 5 minutes and sonicated for 10 minutes at room temperature. The samples were centrifuged at $2700 \times g$ for 30 minutes and the supernatants were transferred to a new set of tubes. Extraction recoveries were determined by liquid scintillation counting (LSC).

A urine or bile sample was pooled across time intervals to generate 0-168 hour sample. Approximately 1 g of each sample was combined with 3 mL of 0.1% formic acid in acetonitrile. The extraction procedure was same as that of plasma as described above and reconstituted with 500 μl water:acetonitrile (1:2.3, v/v). Pooled fecal samples were extracted as described fro plasma samples.

**Metabolite profiling and identification**

Sample analysis was performed on Accela HPLC and connected to Lumos Orbitrap (Thermo Scientific, San Jose, CA). Liquid chromatography was performed with a Polaris C18-A, $4.6 \times 150$ mm, 3 μm (Agilent Technologies, Santa Clara, CA) with mobile phases 10 mM ammonium acetate in water with 0.1% formic acid (mobile phase A) and acetonitrile (mobile phase B). The flow rate was 1 ml/min with 10:1 post column split. The gradient used was: initial hold at 5% B for 2 min, ramp to 40% B at 15 min, hold at 40% B until 28 min, ramp to 50% B at 28.1 min, hold at 50% B until 50 min, and then ramp to 95% B at 54 min, hold until 57 min and return to initial equilibrium conditions.

The protonated molecular ions ($[M+H]^+$) for analytes were determined from full scan mass spectrometric (MS) data acquired using an Orbitrap high-resolution mass

spectrometer equipped with an electrospray ionization source (Thermo Scientific, San Jose, CA). The electrospray voltage was set at 4.0 kV and capillary temperature was 270$^{o}$C. The full-scan mass spectra were obtained at resolving power of 30,000 with accurate mass measurements using external calibration. The corresponding data dependent tandem mass spectrometry (MS/MS) scans acquired at a resolving power of 7,500 with collision induced dissociation.

Radioactivity was analyzed in fractions of LC-MS. The column effluent was collected into DeepWell LumaPlate™-96 microplates (PerkinElmer). Each fraction was collected for 10 seconds of the radioprofile. The fractions were evaporated to dryness and radioactivity in each well was counted using a TopCount NXT™ scintillation and luminescence counter for 5 minutes (urine, bile, feces) and 10 minutes (plasma) at 20°C. HPLC radiochromatograms were reconstructed using the LSC import function in Laura evaluation software (LabLogic Systems; Brandon, FL). The % radioactive peaks were converted to percentages of the dose by multiplying the percentage of administered radioactivity recovered in urine, bile, feces and extraction recovery. Pico-Fluor 40 Carbon-14 cocktail for liquid scintillation counting (LSC) was purchased from PerkinElmer (Waltham, MA).

**Metabolite Profiles in monkeys following oral administration of [$^{14}$C]GDC-0810**

The predominant elimination route of radioactivity from intact female monkeys after an oral dose of [$^{14}$C]**GDC-0810** was feces representing >85% of dose. Urine excretion was a minor route of elimination accounting for only 0.3% of the dose. The overall total mean recovery through 168 hours postdose was 87.2%. Biliary excretion from BDC group accounted for a mean of 47.9% of the dose through 168 hours postdose, whereas fecal excretion accounted for an average of 27.1%.

There are three major radioactive compounds in monkey plasma detected by LC/MS analysis: parent **GDC-0810**, **M6**, and **M3** from organic extracts of plasma samples (Figure 1). Parent was the major component in 0-24 h pool plasma but the acyl glucuronide **M6** became the major circulating component at later time point. M3, the oxidative di-glucuronide, was also a prominent metabolite in monkey plasma.

Each of the radioactive peaks identified from urine was < 0.15% of the dose. **GDC-0810** and the following metabolites were identified: **M3** (oxidative di-glucuronide), **M11** (cysteine, glucuronide conjugation), **M5** (oxidative glucuronide), and **M6** (**GDC-0810** acyl glucuronide).

Approximately 47.9% of the administered dose recovered in bile through 168 hours post dose. Major metabolites observed were **M6**, and **M5**, which accounted for 34.1% and 7.1% of the dose respectively. The other metabolites included **M3** (oxidative di-glucuronide), and **M7** (oxidation) accounting for 1.2%, and 1.0% of the administered dose, respectively. Other minor metabolites were M5d (oxidative glucuronide), **M11** (cysteine, glucuronide conjugation), and **M12** (glucuronide) accounting less than 1.0%

of the administered dose. **GDC-0810** was a minor component in the bile and accounted for around 0.3% of the administered dose.

Fecal excretion was the main route of elimination of **GDC-0810** related radioactivity, with 81.5% and 23.5% of the administered dose recovered in feces through 168 hours post dose in intact and BDC monkeys respectively. No other major metabolites were observed presumably due to hydrolysis of the glucuronide conjugates by the microbial flora in the intestines.

**Metabolite Identification of GDC-0810**

The $[M + H]^+$ and major product ions observed by high resolution full scan and MS/MS experiments for **GDC-0810** and its metabolites are listed in Table 2. A scheme of the proposed metabolic pathways of **GDC-0810** in monkeys and humans is presented in Figure S1.

GDC-0810: The radioactive peak of **GDC-0810** was observed in plasma, urine, and feces. The protonated molecular ion was observed at *m/z* 447. The mass spectra showed product ions at *m/z* 429 (loss of $H_2O$), 311 (loss of indazole and $H_2O$), 299 (loss of phenyl propenoic acid), 284, 263, 169, and 143. The fragmentation pattern of **GDC-0810** observed in study samples was similar to that of the standard. The elemental composition of **GDC-0810** was confirmed using accurate mass analysis.

M1: The radioactive peak of **M1** was observed in plasma. The protonated molecular ion was observed at *m/z* 799. The mass spectra showed product ions at *m/z* 623 (loss of anhydro glucuronic acid), 447 (loss of anhydro glucuronic acid from 623), and 299 (loss of phenyl propenoic acid). The elemental composition of **M1** was confirmed using accurate mass analysis (Table 9). Based on these data, **M1** was tentatively identified as glucuronide of **M6**. Identity of **M1** was also established by comparing the retention time with human cold plasma sample (data not shown).

M3: The radioactive peak of **M3** was observed in plasma, urine and bile. The protonated molecular ion was observed at *m/z* 815. The mass spectra showed product ions at *m/z* 797 (loss of $H_2O$), 639 (loss of anhydro glucuronic acid), 621 (loss of $H_2O$ from 639), 463 (loss of anhydro glucuronic acid from 639), 445 (loss of $H_2O$ from 463), 315 (loss of phenyl propenoic acid), 311 (loss of indazole and $H_2O$). The presence of *m/z* 315 along with 311 suggests that the oxidation occurred on the indazole part of the molecule .The elemental composition of **M3** was confirmed using accurate mass analysis (Table 9). Based on these data, **M3** was tentatively identified as oxidative-**GDC-0810** di-glucuronide conjugate.

M5: The radioactive peak of M5 was observed in plasma, and urine. The protonated molecular ion was observed at *m/z* 639. The mass spectra showed product ions at *m/z*, 463 (loss of anhydro glucuronic acid), 446, 315 (loss of phenyl propenoic acid), 311 (loss of indazole and $H_2O$), 185 and 143. The elemental composition of M5d was confirmed using accurate mass analysis. The presence of *m/z* 315 along with 311

suggests that the oxidation occurred on the indazole part of the molecule. Based on these data, M5 was tentatively identified as oxidative-**GDC-0810** glucuronide conjugate.

M4: The radioactive peak of **M4** was observed in plasma, and bile. The protonated molecular ion was observed at *m/z* 623. The mass spectra showed product ions at *m/z*, 605 (loss of $H_2O$), 447 (loss of anhydro glucuronic acid), 311 (loss of indazole and $H_2O$), and 299 (loss of phenyl propenoic acid). The elemental composition of **M4** was confirmed using accurate mass analysis (Table 9). By comparing with LC/MS analysis of the standard N-glucuronide, **M4** was identified as **GDC-0810** N-glucuronide conjugate.

**Figure S1. Metabolic pathways of GDC-0810 in monkeys**

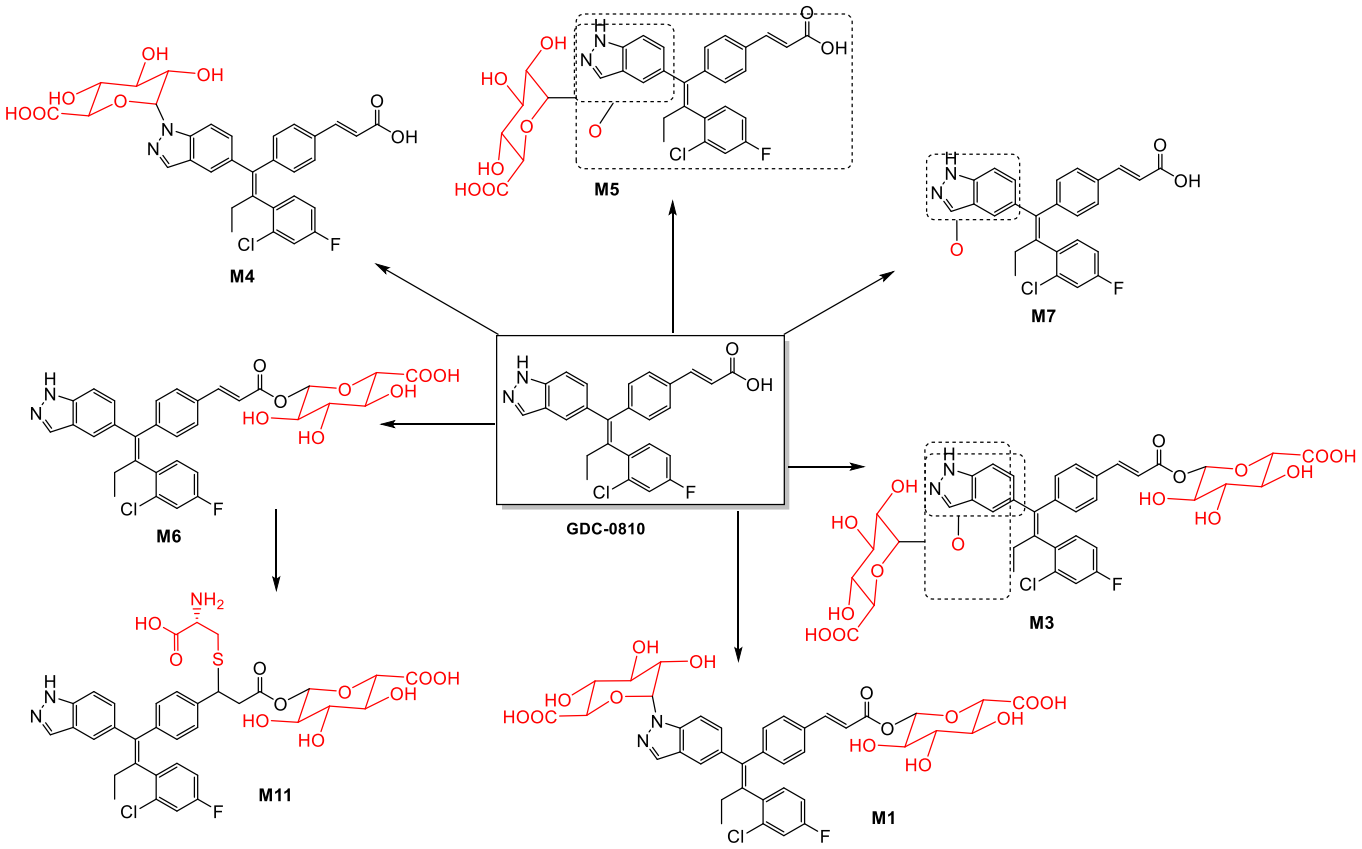

**Figure S2. Radioactivity profiles of urine, bile, and feces following oral dose of [$^{14}$C]GDC-0810**

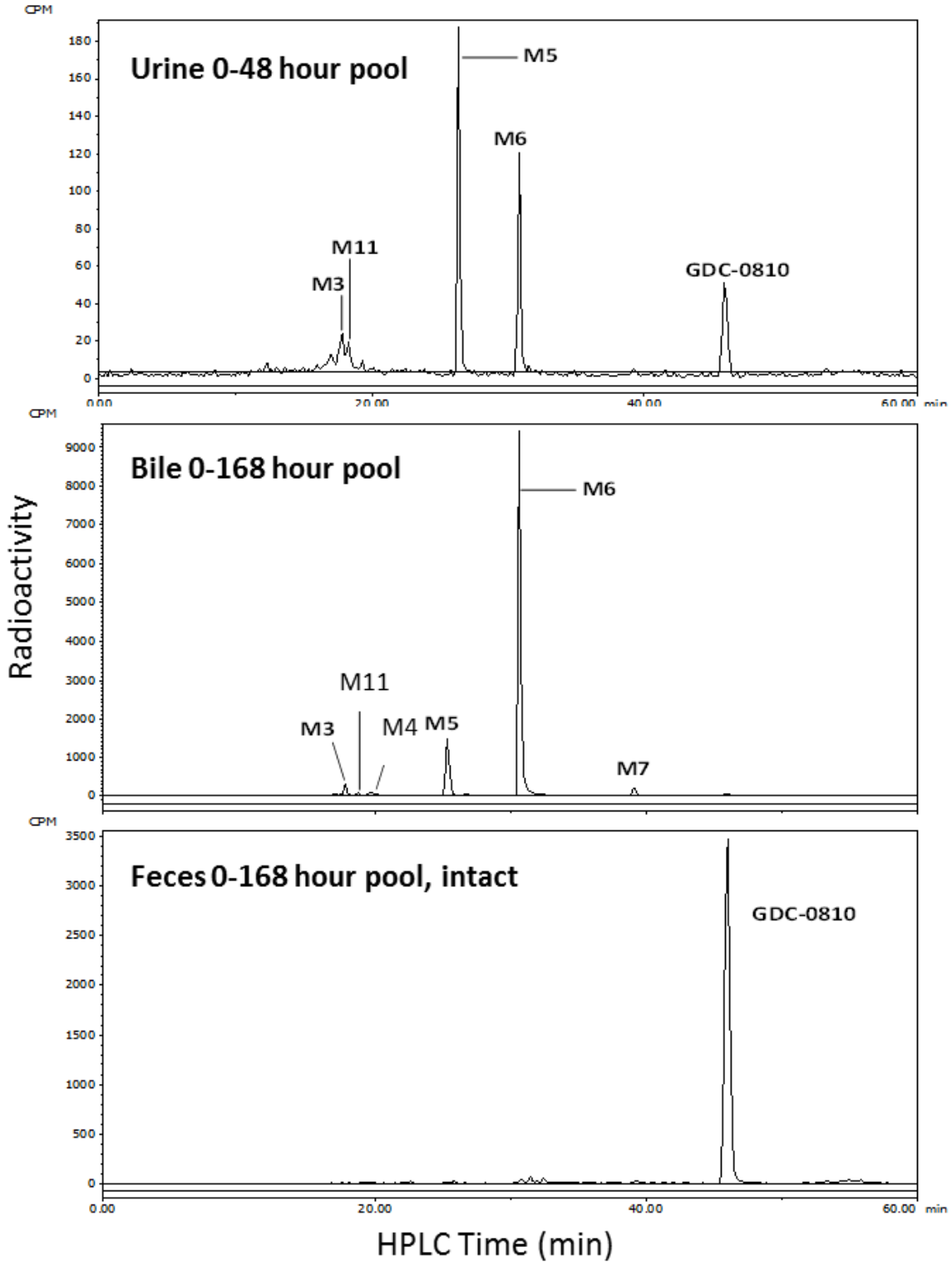

**Figure S3. MS/MS spectrum of M6 of GDC-0810**

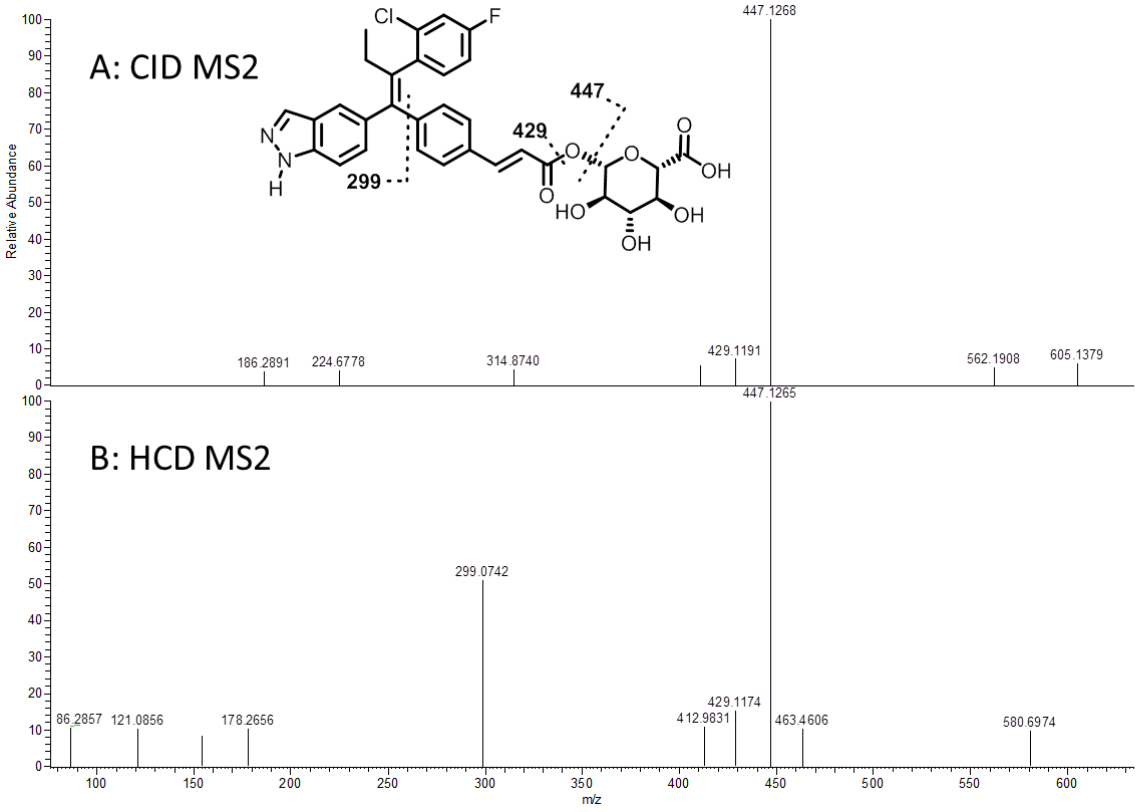

## Figure S4. Product Identification of GSH Adduct of M6 after Glucuronidase Treatment

### A. Before Treatment

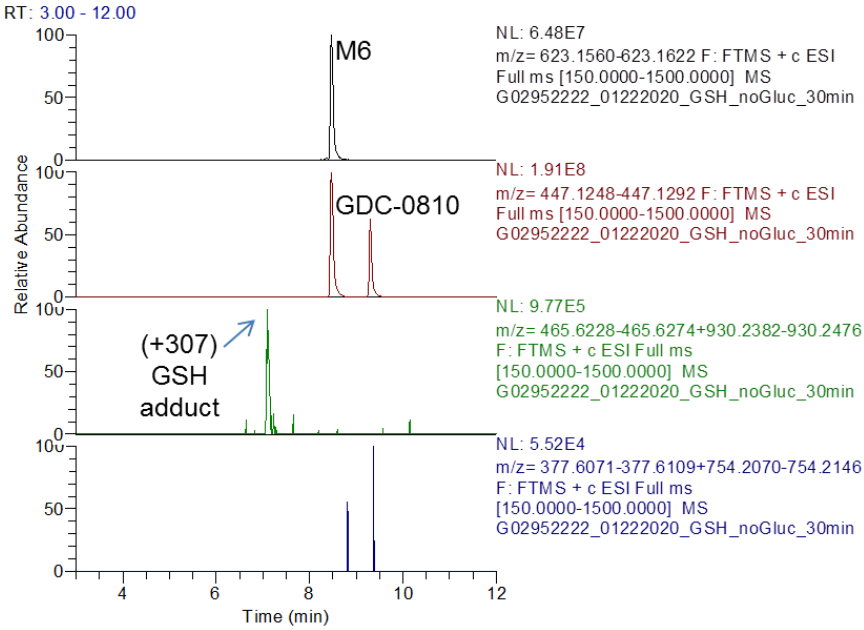


### B. After Treatment

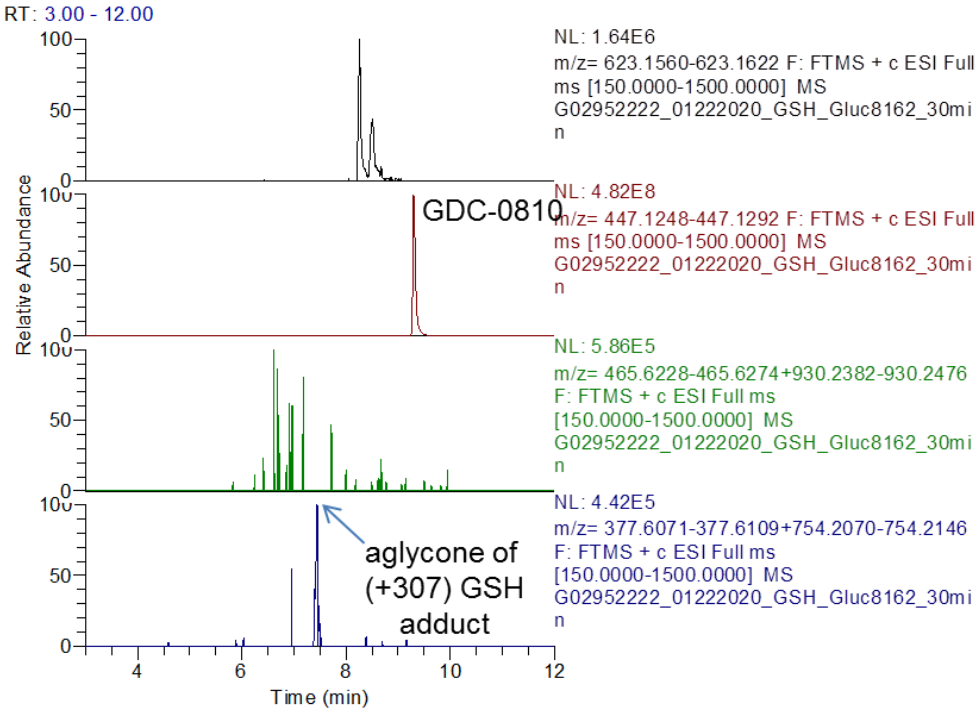

**Table S1. Metabolite characterization of GDC-0810 in monkeys following oral administration**

| Analyte | RT[a] (min) | $[M+H]^+$ (*m/z*) | Proposed Structure and MS/MS Product Ions | Matrix [b] | Major Fragment Ions (*m/z*) |
|---|---|---|---|---|---|
| M1 | 19.0 | 799.1912 | 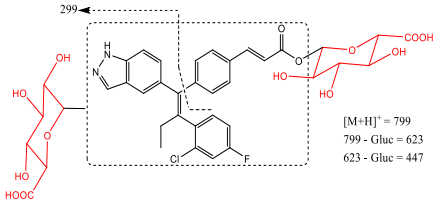 | P, B | 623.1592, 447.1270, 299.0751 |
| M3 | 17.6 | 815.1861 | 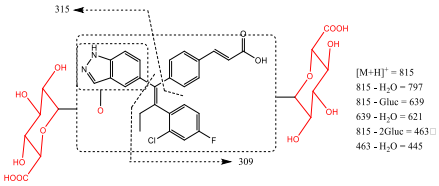 | P, U, B, F | 797.1779,639.1554,621.1442,463.1226,445.1122,315.0706,309.0477 |
| M5 | 18.5 | 639.1540 | 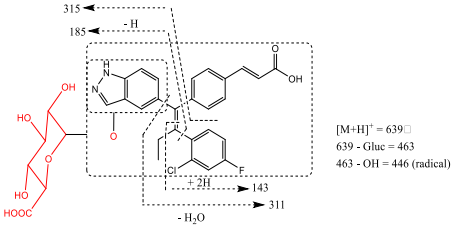 | P, B | 463.12277, 446.1213, 315.0707,311.0633,185.0709,143.0058 |
| M6 | 32.0 | 623.1591 | 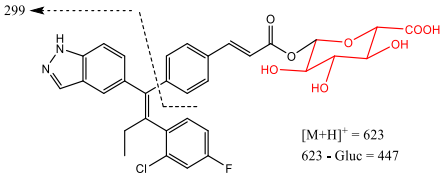 | P, U, B, F | 447.1288, 299.0761 |
| M7 | 43.4 | 463.1219 | 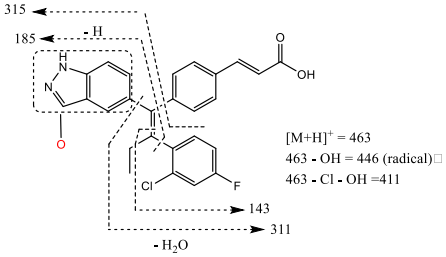 | P, U, B, F | 446.1206, 411.1515, 315.0708, 311.0648, 185.0709, 143.0059 |
| M11 | 18.5 | 744.1788 | 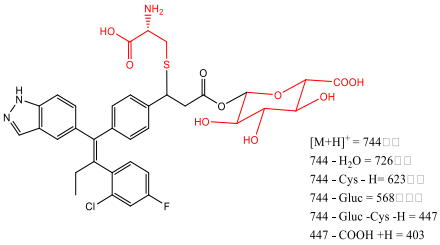 | P, U, B, F | 726.1737,623.1591,568.1501,447.1300,403.1398 |

| | | | | | |
|---|---|---|---|---|---|
| GDC-0810 | 50.3 | 447.1<br>270 | 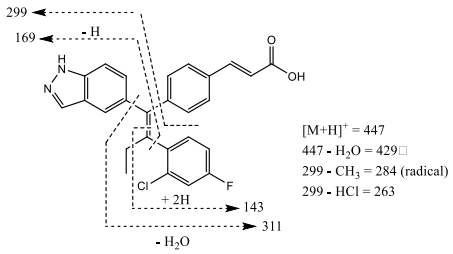 | P, U, B, F | 429.1173,<br>311.0639,<br>299.0753,<br>284.0516,<br>263.0986,<br>169.0760,<br>143.0056 |

$[M + H]^+$ = protonated molecular ion; min = minutes; *m/z* = mass-to-charge ratio;
P= plasma; U= urine; B = bile; F = feces; ppm = parts per million; RT = retention time (min)

[a] Some retention time shift was observed for different species and/or matrices.

[b] Sample matrix containing the metabolite

## Table S2. Coordinates and Energies of Computational Models

**A** (singlet, charge = -1)

| | | | |
|---|---|---|---|
| O | -4.0298876 | 1.2223387 | -0.0001282 |
| C | -3.7503036 | -0.0049503 | -0.0000192 |
| C | -2.2873286 | -0.4067203 | 0.0000138 |
| C | -1.2893816 | 0.4864087 | -0.0000182 |
| C | 0.1583324 | 0.2089947 | 0.0000178 |
| C | 1.0509954 | 1.2905887 | 0.0000578 |
| C | 2.4303834 | 1.0873117 | 0.0000408 |
| C | 2.9438374 | -0.2085293 | -0.0000202 |
| C | 2.0664394 | -1.2964923 | -0.0000602 |
| C | 0.6904184 | -1.0910453 | -0.0000332 |
| O | -4.5728546 | -0.9613503 | 0.0001068 |
| H | -2.0986976 | -1.4786283 | 0.0000548 |
| H | -1.5694156 | 1.5400387 | -0.0000012 |
| H | 0.6547524 | 2.3035427 | 0.0001158 |
| H | 3.1016514 | 1.9412577 | 0.0000718 |
| H | 4.0173824 | -0.3729603 | -0.0000282 |
| H | 2.4580924 | -2.3097913 | -0.0001022 |
| H | 0.0255844 | -1.9500133 | -0.0000692 |

M06-2X/6-31G(d) energy = -497.58025967 Hartree
M06-2X/6-311+G(2df,2p) energy = -497.740001 Hartree
HOMO = -7.61 eV
LUMO = -0.65 eV

---

**B** (singlet, charge = -1)

| | | | |
|---|---|---|---|
| O | 2.1281606 | -2.7367388 | 0.4456974 |
| C | 2.5871906 | -1.5497738 | -0.1652836 |
| C | 4.0496376 | -1.2936138 | 0.1624944 |
| C | 4.4975156 | 0.0603312 | -0.3602046 |
| C | 3.5489446 | 1.1464612 | 0.1775454 |
| C | 3.9294856 | 2.5477122 | -0.3590296 |
| O | 5.1713016 | 2.7968022 | -0.2907886 |
| O | 3.0337456 | 3.2969422 | -0.7818626 |
| O | 2.2152816 | 0.8254262 | -0.1891356 |
| O | 5.8287146 | 0.2590982 | 0.0620914 |
| O | 4.7894516 | -2.3621618 | -0.4016146 |
| C | 1.7697516 | -0.3836068 | 0.3675874 |
| O | 0.4363646 | -0.5576898 | -0.0553346 |
| C | -0.5197674 | 0.1034862 | 0.6453074 |
| C | -1.8501464 | -0.1265058 | 0.0541464 |
| C | -2.9290464 | 0.4532682 | 0.6028564 |
| C | -4.3184474 | 0.3425392 | 0.1455334 |
| C | -4.6966094 | -0.4445668 | -0.9547026 |
| C | -6.0279994 | -0.5112348 | -1.3482026 |
| C | -7.0050654 | 0.2060432 | -0.6514246 |
| C | -6.6423864 | 0.9898242 | 0.4428044 |
| C | -5.3078474 | 1.0559762 | 0.8375254 |
| O | -0.2749844 | 0.7780812 | 1.6223164 |
| H | 2.7684556 | -3.4364588 | 0.2358674 |
| H | 2.4570346 | -1.5953688 | -1.2571456 |
| H | 4.1698036 | -1.2963708 | 1.2584104 |
| H | 4.4347096 | 0.0566522 | -1.4614166 |
| H | 3.6374036 | 1.1771602 | 1.2774894 |
| H | 5.9690166 | 1.2320672 | -0.0340276 |
| H | 5.7217126 | -2.2408298 | -0.1606036 |
| H | 1.8067086 | -0.3444728 | 1.4650774 |
| H | -1.8890074 | -0.7636488 | -0.8230756 |
| H | -2.7665794 | 1.0790022 | 1.4806984 |
| H | -3.9496704 | -1.0080598 | -1.5060726 |
| H | -6.3074094 | -1.1224468 | -2.2010416 |
| H | -8.0441344 | 0.1520192 | -0.9626216 |
| H | -7.3967474 | 1.5483622 | 0.9886714 |
| H | -5.0245404 | 1.6662932 | 1.6914694 |

M06-2X/6-31G(d) energy = -1182.163855 Hartree
M06-2X/6-311+G(2df,2p) energy = -1182.569231 Hartree
HOMO = -8.02 eV
LUMO = -1.35 eV